https://doi.org/10.1016/j.ijbiomac.2024.135308

A NRAS mRNA G-quadruplex Structure-Targeting Small-Molecule Ligand Reactivating DNA Damage Response in Human Cancer Cells for Combination Therapy with Clinical PI3K Inhibitors

Ka-Hin Chan[1], Bo-Xin Zheng[1], Alan Siu-Lun Leung[1], Wei Long[1], Yuchen Zhao[1], Yingying Zheng[1], and Wing-Leung Wong[1,*]

[1] State Key Laboratory of Chemical Biology and Drug Discovery, Department of Applied Biology and Chemical Technology, The Hong Kong Polytechnic University, Hung Hom, Kowloon, Hong Kong SAR 999077, China.

* Corresponding author

E-mail: wing.leung.wong@polyu.edu.hk

Abstract

The *Neuroblastoma RAS (NRAS)* oncogene homologue plays crucial roles in diverse cellular processes such as cell proliferation, survival, and differentiation. Several strategies have been developed to inhibit NRAS or its downstream effectors; however, there is no effective drug available to treat NRAS-driven cancers and thus new approaches are needed to be established. The mRNA sequence expressing NRAS containing several guanine(G)-rich regions may form quadruplex structures (G4s) and regulate NRAS translation. Therefore, targeting NRAS mRNA G4s to repress NRAS expression at translational level with ligands may be a feasible strategy against NRAS-driven cancers but it is underexplored. We reported herein a NRAS mRNA G4-targeting ligand, **B3C**, specifically localized in cytoplasm in HeLa cells. It effectively downregulates NRAS proteins, reactivates the DNA damage response (DDR), causes cell cycle arrest in G_2/M phase, and induces apoptosis and senescence. Moreover, combination therapy with NARS mRNA G4-targeting ligands and clinical PI3K inhibitors for cancer cells inhibition treatment is unexplored, and we demonstrated that **B3C** combining with PI3Ki (pictilisib (GDC-0941)) showed potent antiproliferation activity against HeLa cells (IC_{50}=1.03 μM (combined with 10 μM PI3Ki) and 0.42 μM (combined with 20 μM PI3Ki)) and exhibited strong synergistic effects in inhibiting cell proliferation. This study provides new insights into drug discovery against RAS-driven cancers using this conceptually new combination therapy strategy.

Introduction

The neuroblastoma RAS (*NRAS)* is a proton-oncogene and belongs to the superfamily of three RAS oncogenes, termed as *NRAS*, *KRAS*, and *HRAS*, which encode highly homologous monomeric small guanosine triphosphate (GTP)-binding proteins (20-25 kDa) that play crucial roles as molecular switches to govern the activation of a network of signaling pathways.[1-3] The RAS-guanosine diphosphate (RAS-GDP) is transformed to RAS-guanosine triphosphate (RAS-GTP) when it is catalyzed by guanine nucleotide exchange factors (GEFs), in which RAS-GTP is known as the active form for transmitting signals to activate downstream effector pathways, such as mitogen-activated protein kinase (MAPK) and phosphatidylinositol 3-kinase (PI3K) pathways for cell growth, proliferation and differentiation.[4-7] Under normal conditions, RAS-GTP is exchanged back to RAS-GDP upon hydrolyzed by GTPase-accelerating proteins (GAPs) to terminate the signaling.[1, 8, 9] However, the mutated RAS, such as the predominantly mutation Q61R (CAA to CGA) and Q61K (CAA to AAA) in *NRAS*, produces the mutant NRAS that shows extremely high binding affinity towards GTP and impairs the GTP to GDP hydrolysis.[5, 10] Therefore, the proteins are locked into an activated state and keep transmitting signals to the nucleus for abnormal cell proliferation.[9] RAS is thus a crucial target for anticancer study. Recently, the FDA approved drugs, Sotorasib (AMG510) and Adagrasib (MRTX-849), have been released for treating KRAS G12C specifically;[11, 12] however, NRAS mutated human malignancies do not have any approved inhibitors for clinical use.[13] Despite some indirect approaches utilizing the MAPK inhibitor or PI3K inhibitor to block NRAS downstream signaling pathways have entered clinical trials, these compounds are generally not able to offer desirable inhibition efficiency when they are being used alone. Also, some may show high toxicity in combination therapy with several inhibitors.[14] At present, NRAS mutated human malignancies are still considered as undruggable.[15-17]

G-quadruplexes (G4s) are a class of thermodynamically stable non-canonical secondary structures of RNA and DNA formed by guanine (G)-rich nucleic acid sequences.[18] The stacking of two or more square-planar G-quartets formed via Hoogsteen hydrogen bonding is able to fold

into a G4 structure, which can be further stabilized by the complexed monovalent cations such as potassium ion and other ions.[19] Accumulating *in vitro* and *in vivo* evidences suggest that RNA G4s may play important roles in the regulation of essential biological processes including the expression of cancer related proteins.[20-23] Therefore, RNA G4s are considered as vital molecular targets for chemical biology and drug discovery against cancers and other human diseases.[20-23] Recent studies have revealed that the human *NRAS* proto-oncogene mRNA contains G-rich sequences (e.g. *5'*-GGGAGGGGCGGGUCUGGG-*3'*) in the *5'*-untranslated region (*5'*-UTR).[21, 24] In addition, several reports have demonstrated that G-rich NRAS mRNA sequences may fold into parallel G4-structures, which are potential drug targets of small-molecule ligands.[25, 26] The stabilization of NRAS mRNA G4s with potent ligands may repress NRAS protein expression at translational level in cancer cells.[25-27] Nonetheless, the development of potent small-molecule ligands selectively targeting NRAS mRNA G4s in cytoplasm of living cancer cells remains challenging.

In the present study, we reported a novel fluorescent small-molecule ligand (**B3C**) that exhibited high selectivity and affinity binding to NRAS mRNA G4s. Live-cell imaging also showed that **B3C** was primarily localized in cytoplasm in living human HeLa cells. In addition, the treatment of **B3C** in HeLa cells remarkably downregulated the translation of NRAS, inhibited the NRAS-related biofunctions, arrested cell cycle in G_2/M phase, and induced apoptosis and senescence in a dose-dependent manner. Moreover, **B3C** showed antiproliferative ability against HeLa cells (IC_{50} = 7.6 μM) while at least 6-fold lower antiproliferative ability against noncancerous human cells was observed (HFF1: IC_{50} > 50 μM; BJ: IC_{50} > 50 μM). Furthermore, the inhibition mechanism of **B3C** was investigated comprehensively. We reported herein that repressing NRAS expression at translational level with a NRAS mRNA G4-targeting ligand could reactivate markedly DNA damage response (DDR) that was suppressed by NRAS in HeLa cells. Also, when **B3C** combined with a clinical PI3K inhibitor (GDC0941),[28] it exhibited strong synergistic effects in inhibiting HeLa cell proliferation (IC_{50} = 1.03 μM when combined with 10 μM PI3Ki; and 0.42 μM when combined with 20 μM PI3Ki), indicating that the ligand could be utilized for combination therapy with clinically

used drugs. The present study may provide significant insights into chemical biology study and drug discovery using NRAS mRNA G4s as potential drug targets and also in the development of novel therapeutics against RAS-driven cancers.

2. Results

2.1. Synthesis of B3C and the study of molecular interaction of the ligand with NRAS mRNA G4-structure *in vitro*

Small-molecule ligands capable of binding to NRAS mRNA G4s and downregulating the NRAS expression are rarely reported currently.[25, 26] We thus attempted to develop a fluorescent turn-on ligand to visualize and investigate its intracellular effects targeting NRAS mRNA G4s for chemical biology and antiproliferation study in living cancer cells. The carbazole moisty is a heteroaromatic ring system present in a range of natural products and is known as pharmacologically active compounds.[29] It was reported that carbazole derivatives may exhibit a high affinity, selectivity, and stability to G4-structures because of its rigid planar scaffold for sufficient π-π interactions.[30-32] We thus synthesized new ligands (**B1C**, **B2C**, and **B3C**) as shown in **Scheme S1**, via a flexible ethylene bridge to integrate a carbazole moiety and a benzothiazole moiety. In the molecular design, we are interested in the modification of an alkyl chain functionalized with different terminal functional groups (carboxylic, amide and hydroxyl group) at the nitrogen atom of the benzothiazole group to enhance the polar interaction and water solubility. We first screened these ligands with live-cell imaging to identify a ligand mainly localized in cytoplasm where the target mRNA G4s located. We observed that only **B3C** (**Figure 1F**) was predominately localized in cytoplasm and showed distinct dot-like fluorescent foci in living HeLa cell (**Figure 2A**). **B1C** is mainly localized in mitochondria and **B2C** has relatively low permeability and weak imaging signal in the cells (**Figure S12**). Nonetheless, these ligands show comparable IC_{50} values against HeLa and HFF1 cell lines (**Table S4** and **Figure S13**).

The *in vitro* interaction of **B3C** with different RNA G4s and other nucleic acids (**Table S1**) was investigated. The ligand in buffer solution shows absorption and emission peaks at λ_{ex} = 468 nm and λ_{em} = 595 nm (**Figure S1-S2**). Fluorescent titrations were then conducted and the results were

shown in **Figure 1A** and **Figure S3**. The intensity of fluorescence of **B3C** (λ_{ex}= 468 nm, λ_{em}= 595 nm) was found increased when it interacted with RNA G4 substrates of *TERRA*, *TRF2*, *VEGF*, *NRAS*, and *KRAS*, and was higher than DNA G4 substrates (*Telo21* and *22AG*) and all other non-G4 nucleic acid substrates tested. The fluorescence titration results suggest that **B3C** may show higher preference to interact with RNA G4s to give enhanced green fluorescent interaction signal compared to other nucleic acid substrates tested. Moreover, the equilibrium binding constant (K_{eq}) estimated with fluorescence titrations shows that **B3C** has strong affinity towards NRAS mRNA G4 (K_{eq} = 1.23×10^6 M^{-1}) (**Figure 1B** and **Figure S4**).

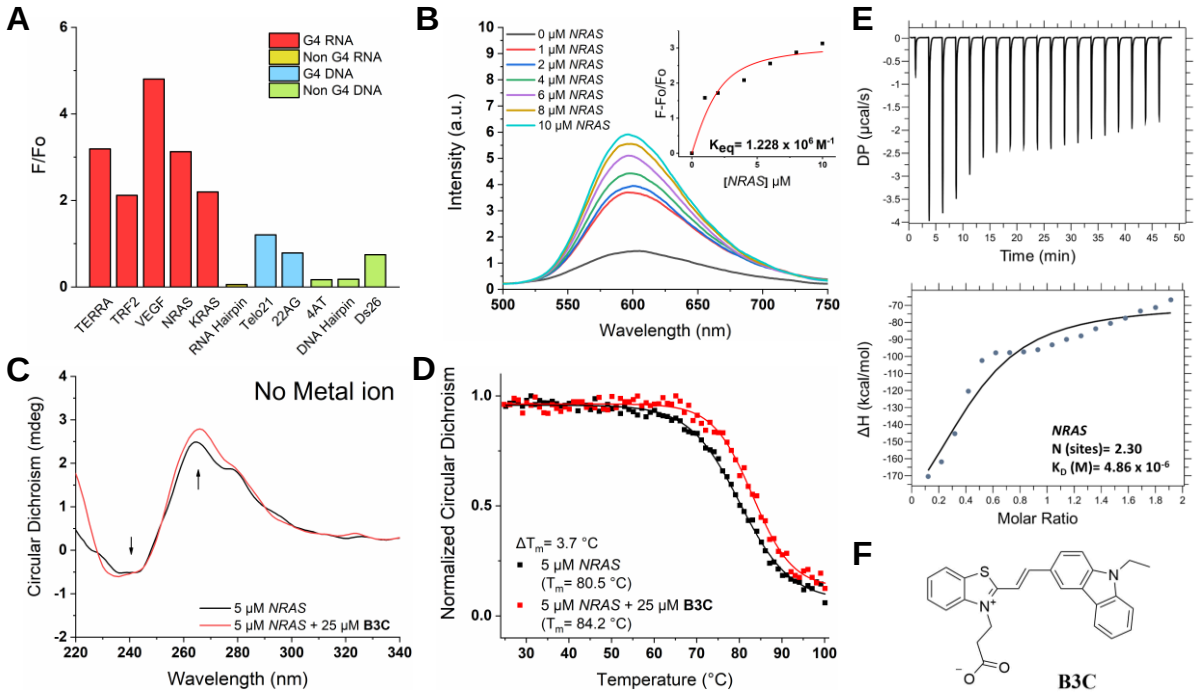

Figure 1. ***In vitro*** **study of the interaction between B3C and different nucleic acid sequences.** (A) Fluorescence titration experiments. The enhanced fluorescence intensity monitored at 595 nm to study the interaction between **B3C** with various G4-RNA, non G4-RNA, G4-DNA, and non-G4 DNA in a pH 7.4 Tris-HCl buffer (10 mM) containing 60 mM KCl. The ligand concentration was 2 μM with nucleic acid substrates at 10 μM. (B) Fluorescence titration spectrum of 2 μM **B3C** with NRAS G4-RNA in a pH 7.4 Tris-HCl buffer (10 mM) containing 60 mM KCl. (C) CD spectrum of NRAS G4-RNA with or without **B3C** (25 μM) in a Tris-HCl buffer (10 mM, pH 7.4) without KCl. (D) CD melting curves for NRAS G4-RNA with or without the addition of **B3C** in a pH 7.4 Tris-HCl buffer (10 mM) containing 60 mM KCl (E) ITC study for the interaction between **B3C** and NRAS G4-RNA in a pH 7.4 KH_2PO_4 buffer solution (25 mM) containing 60 mM KCl. (F) The zwitterionic structure of **B3C**.

In addition, circular dichroism (CD) measurements for the interaction of **B3C** with RNA-G4s under the condition without K^+ ions show that there is an observable increase in the absorption

peaks at 240 nm and 264 nm (**Figure 1C** and **Figure S6**), which indicates that **B3C** may induce the formation of RNA G4s. However, these CD signal changes are not found for **B3C** interacting with DNA G4s. CD thermal denaturation assays were then performed to demonstrate that **B3C** could stabilize RNA G4s (**Figure 1D** and **Figure S8**). The ΔT_m value of **B3C**-TERRA G4 and **B3C**-NRAS G4 complexes was found to be 8.8 and 3.7 °C, which is higher than other RNA G4s. On the contrast, **B3C** does not show stabilization effects with DNA G4s (Telo21 and 22AG), non-G4 DNA (double-stranded DNA, ds26) and non-G4 RNA (Hairpin). Isothermal titration calorimetry (ITC) (**Figure 1E** and **Figure S9**) was also performed to study the interaction of **B3C** with RNA G4s. The affinity (K_d) values suggest that **B3C** exhibits a strong affinity to RNA G4s, notably to NRAS mRNA G4 (K_d = 4.86 μM) and TERRA RNA G4 (K_d = 4.53 μM). The results were found consistent with the ΔT_m analysis. Collectively, these molecular interaction results indicate that **B3C** may selectively interact with RNA G4-structures *in vitro*, particularly NRAS RNA G4 and TERRA RNA G4. Furthermore, the binding stoichiometry for **B3C** interacting with NRAS RNA G4 and TERRA RNA G4 was studied by Job plot analysis (**Figure S10**). The results suggest that two molecules of **B3C** may interact with one G4-structure, which is comparable with ITC analysis that suggests two possible binding sites for the G4-structure (**Table S4**).

Table 1. Half-maximal inhibitory concentration (IC_{50}) of B3C against cancer and noncancerous cell lines.

	Cell lines	IC_{50} (μM)
Cancer cells	HeLa	7.55 ± 0.6
	A2058	25.01 ± 3.1
	HCT116	73.39 ± 23.2[a]
	PANC-1	> 50[b]
Noncancerous cells	HFF1	> 50[b]
	BJ	> 50[b]

[a] The measured IC_{50} was larger than 50 μM (highest dose in MTT assay), so the value was determined by fitting the non-linear fitting curve.

[b] The IC_{50} cannot be fitted in the non-linear fitting curve and the cell viability is higher than 50% at 50 μM **B3C**.

2.2. Antiproliferation effect of B3C and visualization of G4-structures in live HeLa Cells

The cell growth inhibition effect of **B3C** against different cancerous and noncancerous human cell lines was evaluated with MTT assays. The result was summarized in **Table 1** and **Figure S11**. In general, **B3C** exhibits higher toxicity against cancer cells compared to the noncancerous cells tested. In addition, HeLa cells were found more susceptible to **B3C** (IC_{50} = 7.6 μM), while the IC_{50} values for human noncancerous fibroblast cells, HFF1 and BJ, were found over 50 μM. The result suggests that **B3C** may be a potential antiproliferative agent against HeLa cells and it has a relatively low toxicity against noncancerous cells.

To understand better the possible intracellular targets of **B3C** in living human cells, we performed live-cell imaging in HeLa cells. From **Figure 2A**, the green foci observed in the **B3C**-treated cells clearly illustrate that **B3C** is primarily localized in cytoplasm but not in nucleus. To further verify the target imaged with **B3C** in cytoplasmic region was not mitochondria, colocalization imaging of **B3C** with Mito-Tracker, a commercial mitochondria-specific staining agent, was thus performed in living HeLa cells. The confocal images (**Figure 2B**) show that **B3C** (green foci) is not colocalized with Mito-Tracker (red foci), which supports that mitochondria may not be the primary target of **B3C**. In addition, an immunofluorescent imaging was performed to colocalize **B3C** with lysosomal-associated membrane protein 1 (LAMP1), a protein that is localized in cytoplasm. The result shown in **Figure 2C** indicates that green foci (**B3C**) are generally well-colocalized with LAMP1 (red foci) in cytoplasm. Therefore, these cellular imaging results support that **B3C** may primarily localize in cytoplasm in living HeLa cells.

To further verify the intracellular substrate interacted with **B3C** is RNA instead of DNA, enzymatic digestion assays were carried out for **B3C**-treated HeLa cells. The cells after the treatment with RNase A, the green imaged substrates (**B3C**) were almost completely disappeared (**Figure 2E**) compared to the control. However, the green fluorescent signal was not affected when

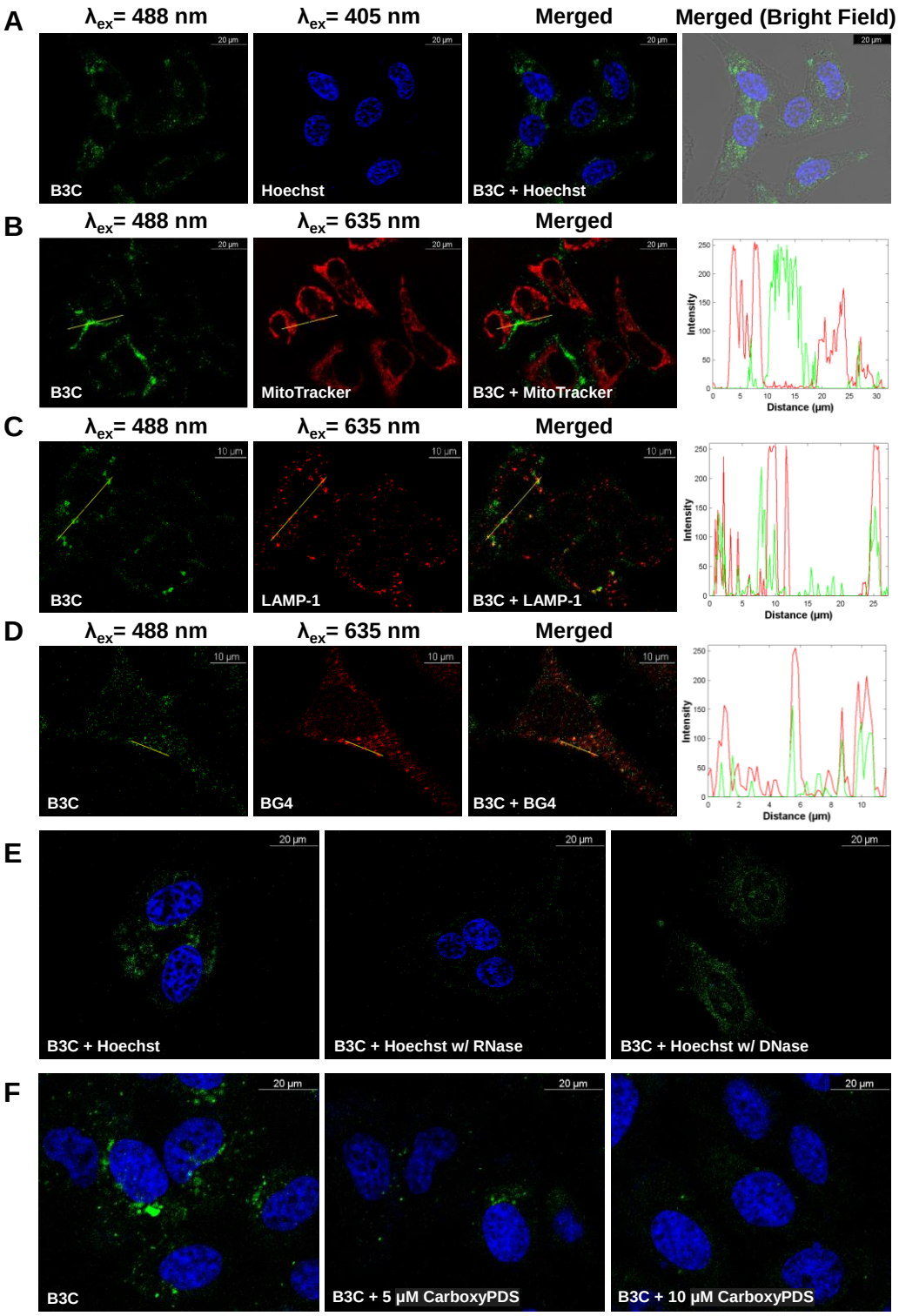

Figure 2. Confocal imaging of B3C in HeLa cell. (A) Confocal live-cell imaging **B3C** (5 μM, 15 min) and Hoechst 33342 (2 μM, 10 min). (B) Confocal co-localization live-cell imaging of **B3C** (5 μM, 15 min) and MitoTacker Deep Red (30 nM, 30 min). (C) Immunofluorescent co-localization imaging of **B3C** (5 μM, 15 min) and lysosome associate membrane protein 1 (LAMP-1). (D) Immunofluorescent co-localization imaging of **B3C** (5 μM, 15 min) and G4 specific antibody, BG4. (E) Confocal enzymatic digestion imaging of fixed HeLa cells with **B3C** (5 μM, 15 min) and DAPI (2 μM, 10 min) with or without RNase A and DNase I treatment. (F) Confocal competitive imaging of **B3C** (5 μM, 15 min) and Hoechst 33342 (2 μM, 10 min) with or without the addition of 5 and 10 μM **CarboxyPDS** (2 h).

the cells were treated with DNase I. The enzymatic digestion result reveals that **B3C** mainly interacts with RNA substrates in HeLa cells and gives green fluorescent signals.

Furthermore, the colocalization study of **B3C** and BG4 (a commercial G4-specific antibody) was performed in fixed cells to illustrate the intracellular target of **B3C** could be RNA G4s. From **Figure 2D**, the green foci (**B3C**) were found mostly well-colocalized with the red fluorescence staining (BG4) in HeLa cells, which supported that **B3C** could possibly interact with RNA G4s in the cells.

To better elucidate that **B3C** interacted with cytoplasmic RNA G4s in cells, we employed three well-known G4-ligands, CarboxyPDS[33, 34], PDS[35-37] and BRACO19[38, 39], for intracellular competition study in living HeLa cells. From **Figure 2F**, for the cells after being treated with RNA-G4 selective CarboxyPDS, the green foci (**B3C**) in live HeLa cells were faded out markedly, which indicated that **B3C** could possibly compete with CarboxyPDS for the same or similar cellular targets that were presumably RNA-G4 structures. The intracellular competition study performed with other well-unknown G4 ligands, PDS and BRACO19, also reduced the fluorescent signal of **B3C** (Figure S14). Taken together, these cellular imaging and competition results suggest that **B3C** may most likely target RNA G4-structures in cytoplasm of living HeLa cells.

2.3. B3C downregulating NRAS expression and reactivating DNA damage response (DDR)

It has been reported that RNA G4-structures may play roles as a translational repressor for different genes to downregulate the expression of corresponding proteins.[21-23] We thus attempted to figure out whether gene expression could be interrupted by **B3C** in HeLa cells. Quantitative real-time RCR (qRT-PCR) was carried out to study the expression of *TERRA, TRF2*, *NRAS*, *KRAS*, and *VEGF* because all these mRNA G4s interacted with **B3C** *in vitro*. As shown in **Figure 3A**, it was observed that there was a significant increase in the expression of *TERRA* and *TRF2* RNA, which were two genes that closely related to telomere and DNA damage.[40-42] These results may indirectly indicate that **B3C** could possibly induce DNA damage. It is noteworthy that no significant change was found on the RNA expression of *NRAS*, *KRAS*, and *VEGF*, which

suggests that **B3C** may not affect the transcriptional process in the cells to express RNA from DNA. It could be due to the primary cellular target of **B3C** is RNA G4-structures but not DNA.

Then, we studied the regulation of **B3C** on the translation of NRAS, TRF2, KRAS, and VEGFA in HeLa cells by western blotting. From **Figure 3B** and **3C**, the results clearly indicates that the expression of NRAS protein was inhibited with **B3C** in a dose-dependent manner. While for TRF2, its protein expression was not repressed but enhanced in the cells treated with **B3C**. These results are in accord with the qRT-PCR results (**Figure 3A**). Furthermore, the downregulation of KRAS and VEGFA was found non-significant in **B3C**-treated cells, probably due to their weak affinity (Table S4). Therefore, these results suggest that **B3C** may selectively interact with NRAS mRNA G4s and repress the translation process in HeLa cells.

To further evaluate the cellular interaction and the effect of **B3C** observed on the downregulation of NRAS expression by targeting its mRNA G4s, dual-luciferase reporter assays were conducted. In the assays, the psiCHECK-2 vectors were constructed by inserting the wildtype NRAS mRNA G4 sequence (WT) or mutant NRAS mRNA G4 sequence (Mut) in front of *Renilla* luciferase coding sequence.[43, 44] When *Firefly* luciferase was used to act as an internal control, no modification was made in front of its coding sequence. From **Figure 3D**, the ratio of *Renilla/Firefly* luciferase activities in the wild type (WT) was found significantly decreased in a dose-dependent manner with **B3C** after 48 h treatment. However, no significant change was observed on the *Renilla/Firefly* luciferase activities in the mutant (Mut). These results clearly show that the treatment of **B3C** inhibits the expression of *Renilla* that is inserted with a wildtype NRAS mRNA G4 sequence. On the contrary, the one with a Mut sequence inserted cannot fold into G4-structures and thus it is not repressed in the assay. The results support that **B3C** may target the inserted wildtype NRAS mRNA G4 sequence and then inhibits the expression of *Renilla* in the cells.

To better understand the inhibition mechanism, RNA immunoprecipitation (RIP) was also performed. DHX36 is a known helicase that unwinds RNA G4s. It has been reported that G4-ligands may inhibit the expression of the corresponding protein by disrupting the RNA G4-DHX36

interaction.[25, 26, 45] Therefore, RNA sequences capable of folding into stable G4-structures under physiological microenvironment may act as a blocking unit to interfere the translation of a mRNA into its corresponding protein. From the result of RIP, shown in **Figure 3E** and **Figure S16**, a significant decrease in the amount of captured NRAS mRNA after the treatment with **B3C** was observed. The results indicate that **B3C** may interfere the recognition of DHX36 to NRAS mRNA G4-structure. Together with the result of dual-luciferase assays, the results support that **B3C** may target NRAS mRNA G4s and stabilize the complex formed *in situ*, and thus it affects the interaction

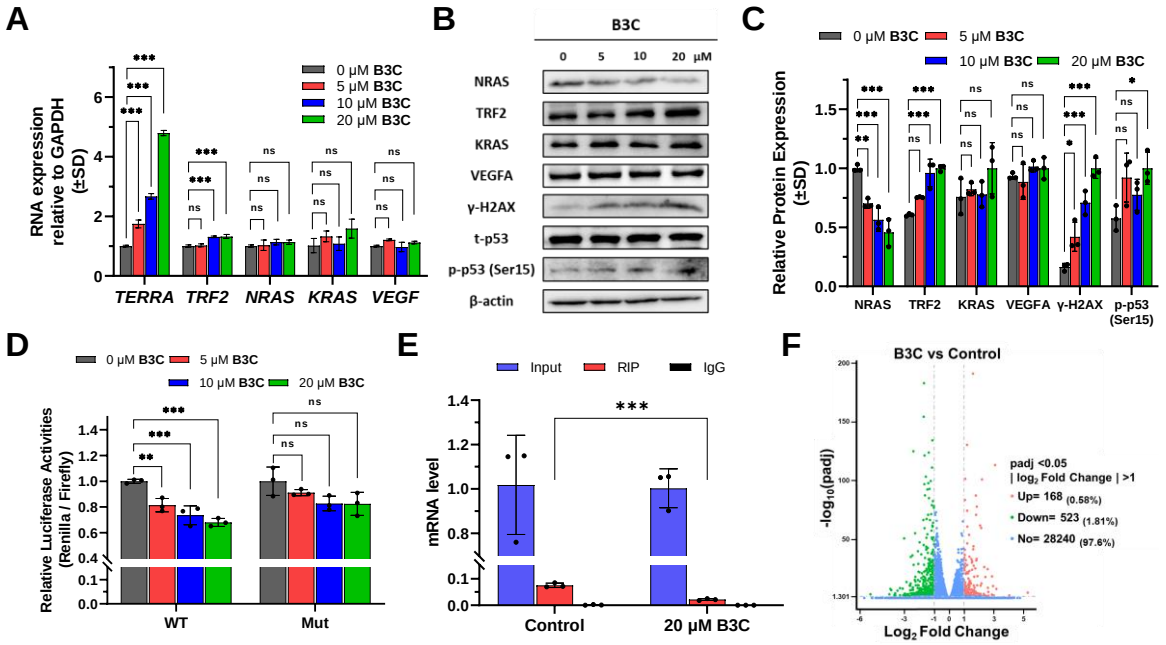

Figure 3. Cellular study on the expression of mRNA and proteins after the treatment of B3C on HeLa cells. (A) The relative transcription of TERRA ncRNA, TRF2 mRNA, NRAS mRNA, KRAS mRNA, and VEGF mRNA in HeLa cells treated with **B3C** (0, 5, 10, and 20 μM) for 48 h, and GAPDH was used as the endogenous control (N=3, mean ± SD). (B) Western blots assay to determine the translation of NRAS, TRF2, KRAS, VEGFA, γ-H2AX, t-p53, phos-p53 (Ser15), and β-actin in HeLa cells treated with **B3C** (0, 5, 10 and 20 μM) for 48 h. (C) The relative proteins expression of HeLa cells after the treatments with **B3C** of different concentration (N=3, mean ± SD). (D) Relative luciferase activity (ratio of *Renilla* luciferase activity to firefly luciferase activity) in psi-CHECK2 vectors containing the NRAS mRNA G4 (WT) or mutated sequence (Mut) upon the treatment of **B3C** (0, 5, 10, and 20 μM) for 24 h. (E) Recruitment of DHX36 to the NRAS mRNA upon the treatment of **B3C** (20 μM) in HeLa cells in the RIP assay. (F) RNA sequencing analysis in HeLa treated without or with **B3C** for 48 h. Details of gene expression data were given in Figure S17 to S19 in Supporting Information.

between DHX36 and NRAS mRNA G4. Consequently, **B3C** hinders DHX36 to unwind NRAS mRNA G4 and eventually may inhibit the expression of NRAS protein.

To get more detailed information on the cellular targets of **B3C**, RNA-sequencing was performed to compare the change of cellular RNA in HeLa cells treated with or without **B3C**. From the volcano plot showed in **Figure 3F**, only about 2.4% of the total genes were affected by **B3C**. These results suggest that the cellular target of **B3C** is concentrated. Moreover, from the qRT-RCR analysis (**Figure 3A**), the results suggest that DNA damage may be induced by **B3C**. Western blot assays were thus performed to investigate the expression level of γ-H2AX. It has been reported that γ-H2AX is regarded as an important molecular marker of DNA damage as it plays an important role in signaling and initiating the repairment of damaged DNA.[46, 47] The western blot results (**Figure 3B**) indicate that there is a significant upregulation on the expression level of γ-H2AX, indicating that DNA damage may be induced in the **B3C**-treated cells.

We have verified that **B3C** is primarily localized in cytoplasm but not in nucleus in living HeLa cells, therefore, it is unexpected that DNA damage is markedly increased in the cells after **B3C** treatment. We thus speculated that reactive oxygen species (ROS) may be one of the direct sources causing DNA damage if the nuclear DNA is not directly impacted by **B3C** in the nucleus.[48, 49] However, out of our expectation, the results obtained from TMRE, MitoROX, and CellROX staining assays evidently suggest that mitochondrial membrane potential was not affected by **B3C** and, more importantly, no significant increasing of ROS level in both mitochondria and cytoplasm was observed (**Figure S20-S22**). These cellular results indicate that **B3C** may not enhance ROS production in HeLa cells and thus DNA damage is not likely a result of induced ROS with the ligand.

NRAS is known closely related to DNA damage. Abulaiti *et al.* reported that the expression of NRAS in cancer cells caused chromosomal instability and the resulting damaged DNA promoted a cell transformation to alter its cell morphology.[50] More importantly, the transformed cells are found to be insensitive to DNA damage because they have a low phosphorylation rate on p53 at Serine 15, which is the site for responding DNA damage.[50-52] Subsequently, the NRAS-expressed cells may not be able to undergo cell cycle arresting and induce γ-H2AX formation despite the existing of chromosome instability.

Because of the suppressing of cells to respond to DNA damage by NRAS, we questioned whether the downregulation of NRAS with **B3C** could restore the ability of the cells to respond to DNA damage via activating DNA damage response (DDR). To address this hypothesis, we then examined the expression of phos-p53 (S15) by western blotting (**Figure 3B**). The result clearly reveals that phos-p53 (S15) was upregulated in the HeLa cells treated with **B3C** for 48 h. Taken together, these results suggest that the downregulation of NRAS with **B3C** may promote the phosphorylation on p53 and reactivate the DDR. Consequently, the γ-H2AX protein can be phosphorylated in order to respond to the damaged DNA in the cells.

2.4. B3C reactivating and mediating the DNA damage respond signal through ATR and ATM pathway and arrested cell cycle

To further elucidate the DNA damage event observed, comet assays were performed to visualize the degree of damaged DNA in HeLa cells before and after **B3C** treatment. From **Figure 4A**, it was found that some HeLa cells (Control, without **B3C** treatment) contain damaged DNA as blue tails were observed. This result is in accord with the previous study that NRAS-expressed cells may cause chromosomal instability.[50] The cells after being treated with **B3C**, both at 10 and 20 μM, HeLa cells showed a more distant and longer blue tail than that of the control (**Figure 4A**). These results support that **B3C** induces DNA damage.

Then, we studied the DNA damage response pathway by performing western blotting on ATR and ATM signaling pathways (**Figure 4B**) to understand how the **B3C**-treated cells respond to the reactivation of DNA damage response.[53, 54] From the result of western blotting (**Figure 4C** and **4D**), it clearly showed that both ATM and ATR pathways were activated as the phosphorylation was upregulated in the cells treated with **B3C** in a dose-dependent manner. At the same time, their downstream effectors, CHK-1 and CHK-2, were also significantly phosphorylated. These results support that the treatment of **B3C** may activate DDR in HeLa cells.

To better understand the relationship between DDR and the inhibition pathway in cell growth, the expression of some downstream effectors was analyzed.[55, 56] The result shows that there

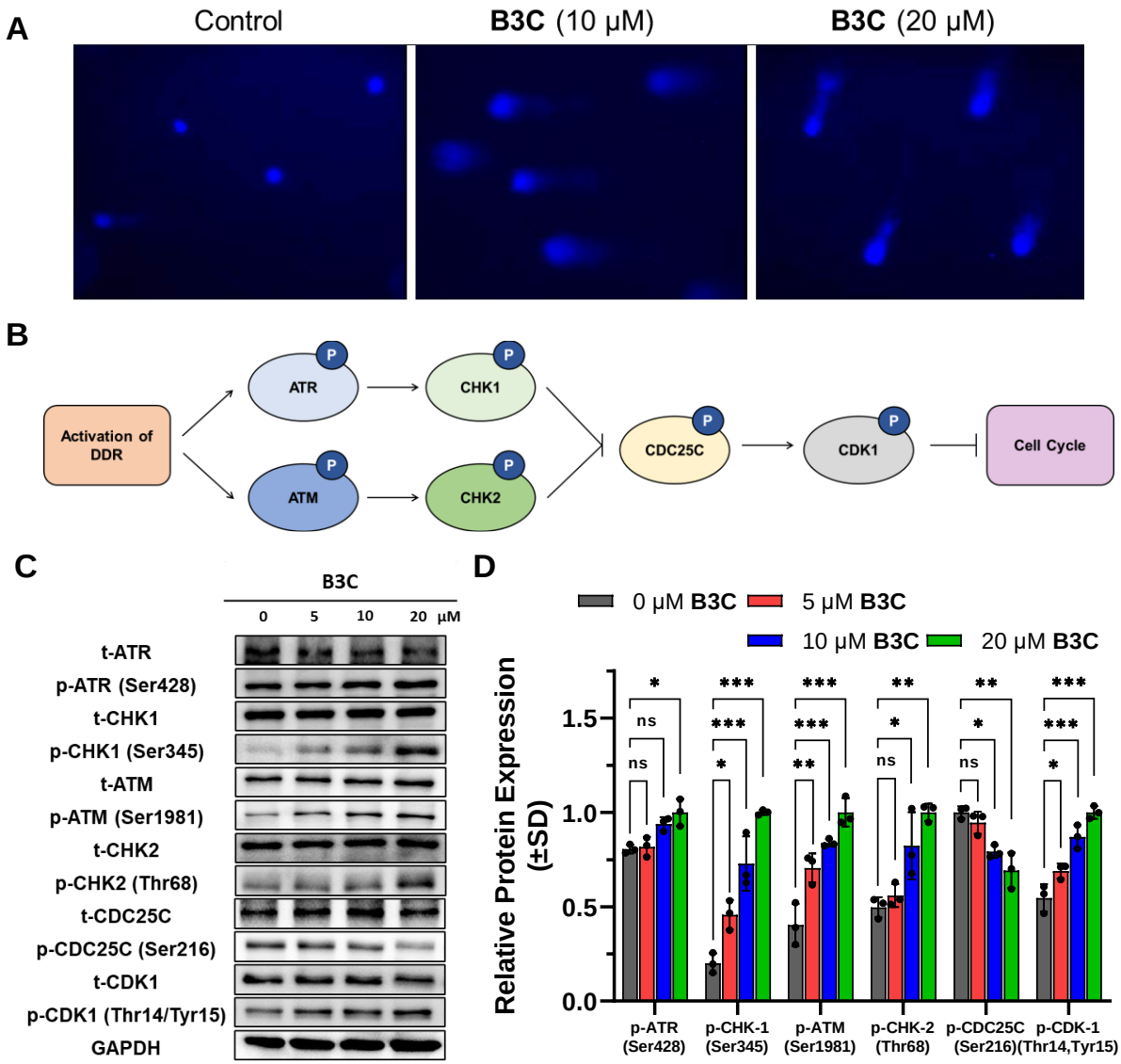

Figure 4. The study on induction of DNA damage and the activation of DNA Damage Response (DDR) after the treatment of B3C on HeLa cells. (A) Comet assay analysis of DNA damage in HeLa cells after 48 h of treatment **B3C** (10 and 20 μM). (B) Schematic diagram of the proteins in ATR and ATM DNA-damage pathways. (C) Western blots assay to determine the activation of DDR pathway by the translation of t-ATR, p-ATR (Ser428), t-CHK1, p-CHK1 (Ser345), t-ATM, p-ATM (Ser1981), t-CHK2, p-CHK2 (Thr68), t-CDC25C, p-CDC25C (Ser216), t-CDK1, p-CDK1 (Thr14/Thy15) and GAPDH in HeLa cells treated with **B3C** (0, 5, 10 and 20 μM) for 48 h. (D) The relative proteins expression of HeLa cells after the treatments with **B3C** of different concentration (N=3, mean ± SD).

was a significant downregulation on the phosphorylation on CDC25C and upregulation on phosphorylation of CDK1. These results indicate that cell cycle arresting may be induced after the reactivation of DDR (ATR and ATM pathway)[57, 58] by downregulating the expression of NRAS with **B3C** and, therefore, HeLa cells growth is inhibited. As CDC25C and CDK1 are two important cell cycle regulators,[58-61] cell cycle analysis was then performed to study the cell cycle of HeLa

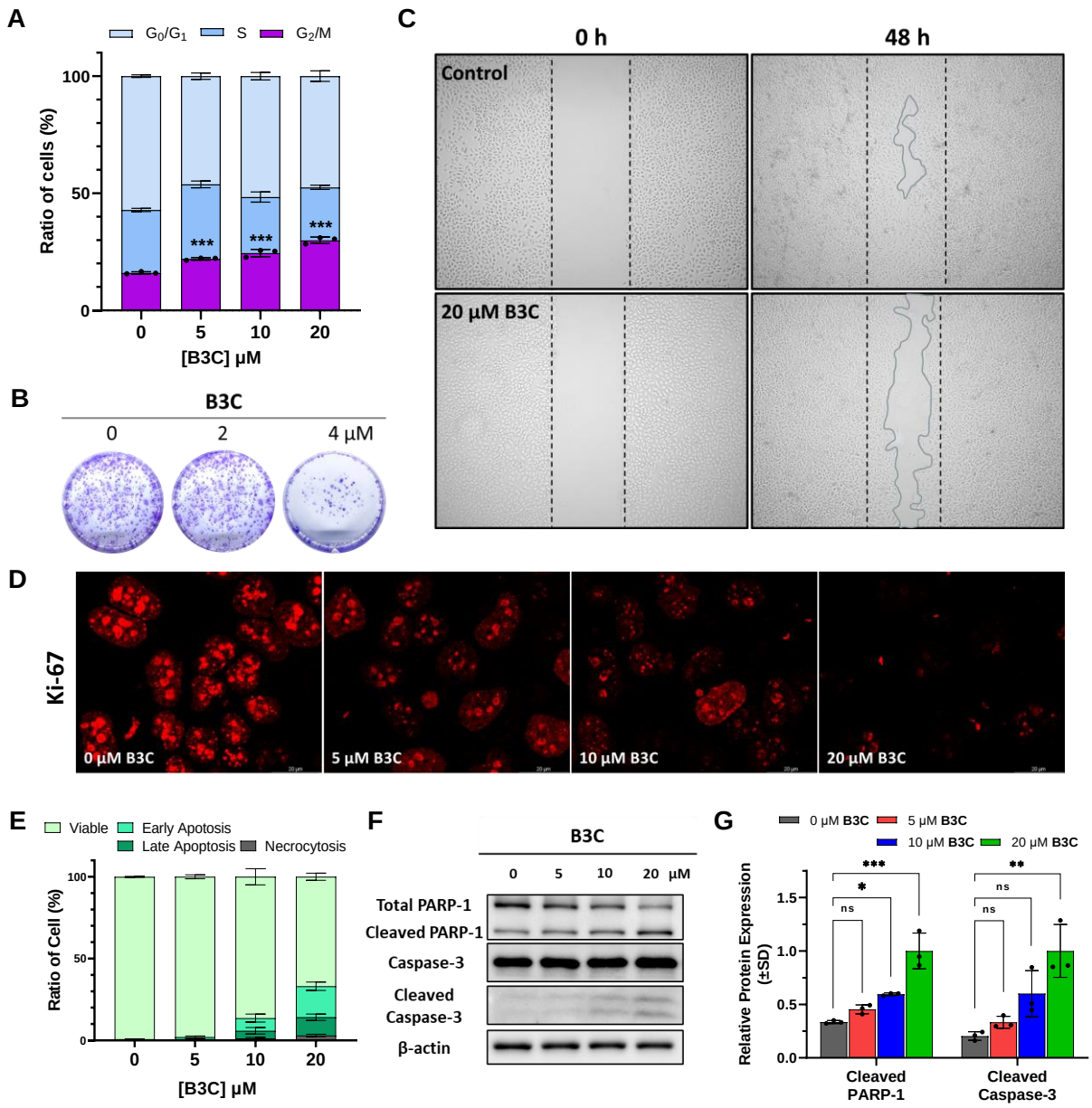

Figure 5. The mechanism of B3C in the inhibition of HeLa cell growth and proliferation. (A) The percentage of HeLa cells in different phases in the cell cycle after the treatments with **B3C** of different concentration (N=3, mean ± SD) for 48 h. (B) Analysis of cell proliferation of HeLa cells by in vitro colony formation assay after the treatment of **B3C** (0, 2, and 4 μM) for 10 days. (C) Analysis of HeLa cells migration by in vitro wound healing assay after the treatment of **B3C** (20 μM) for 48 h. (D) Immunofluorescent imaging of Ki-67 to study the cell proliferation of HeLa cells after **B3C** treatment (0, 5, 10, and 20 μM) for 48 h. (E) The percentage of apoptotic HeLa cells after the treatments with **B3C** of different concentration (N=3, mean ± SD) for 48h. (F) Apoptosis analysis by western blotting to determine the expression of apoptotic proteins, cleaved PARP-1, cleaved caspase-3 in HeLa cells after treating with **B3C** (0, 5, 10 and 20 μM) for 48 h. (G) The percentage of apoptotic HeLa cells after the treatments with **B3C** of different concentration (N=3, mean ± SD).

cells treated with **B3C**. The results illustrate that **B3C** treatment arrested the cell cycle in G_2/M phase in a dose-dependent manner (**Figure 5A** and **Figure S24**). Literatures also suggest that

DNA damage and phosphorylation of p53 may cause G_2/M phase arresting in cell cycle.[62-64] Our results obtained thus far are in good alignment with literature. Since G_2/M phase is being arrested, the proliferation of **B3C**-treated cells is thus inhibited.

2.5. B3C repressing NRAS-related functions and inducing apoptosis and senescence in HeLa cells

The cell proliferative ability for **B3C**-treated HeLa cells was examined by staining the cellular Ki-67 with immunofluorescent experiments.[65] The confocal imaging (**Figure 5D**) showed that the expression of Ki-67 was significantly reduced in a dose-dependent manner, which indicated that the proliferation of **B3C**-treated cells was inhibited. Furthermore, the colony formation assay (**Figure 5B**) was performed to evaluate the proliferation of HeLa cells after **B3C** treatment. It was found that **B3C** at 4 μM almost completely inhibited cell proliferation. **B3C** may also inhibit the migration of HeLa cells (**Figure 5C**). These results are in good alignment with the function of NRAS that promotes the proliferation and migration of cancer cells.[4-7]

The apoptosis in **B3C**-treated HeLa cells was studied with flow cytometry. We found that **B3C** induced apoptosis in a dose-dependent manner from 0.63 % (Control) to 1.84 %, 12.4 %, and 30.9 % for the cells treated with the ligand at 5, 10 and 20 μM for 48 h, respectively (**Figure 5E** and **Figure S25**). Western blotting (**Figure 5F** and **5G**) was also performed to confirm the upregulation of two apoptotic related proteins, Cleaved Poly [ADP-ribose] polymerase 1 (cleaved-PARP-1) and cleaved-caspase 3. However, we found that the population of apoptotic cells observed was not the majority in **B3C**-treated HeLa cells (**Figure 5E**). We thus speculated that **B3C** may have another pathway to inhibit HeLa cell proliferation. Therefore, we performed SA-*β*-gal assays to study whether **B3C** could induce senescence. From **Figure 6A**, the results indicate that **B3C** causes HeLa cell senescence. Then, the senescence pathway was further studied by investigating the development of senescence-associated secretory phenotype (SASP).[66, 67] The expression of SASP related mRNA (*IL-1α*, *IL-6* and *IL-8*) was then studied by qRT-PCR. The

result shows that there were significant upregulations on these mRNA (**Figure 6B**). To further confirm the expression of their corresponding proteins, ELISA were performed on each of these proteins. The result shows that these SASP related proteins were upregulated significantly (**Figure 6C**). Taken together, these results obtained thus far may lead to a conclusion that **B3C** could be able to inhibit the proliferation of HeLa cells by downregulating NRAS expression, inhibiting NRAS-associated functions, and inducing apoptosis and senescence.

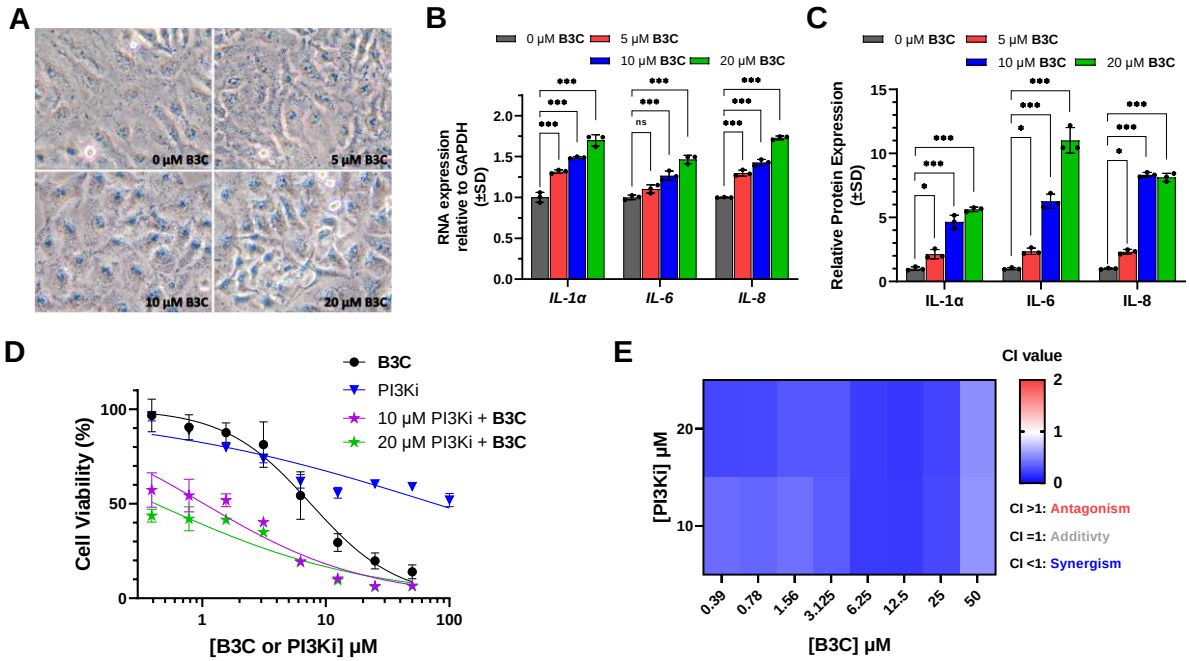

Figure 6. The study on the induction of senescence on B3C treated HeLa cells and the synergetic effects of the combination of B3C and clinical PI3K inhibitor. (A) SA-β-gal assays to investigate the effects of **B3C** on cell senescence of HeLa cells. (B) The relative transcription of SASP related mRNA, *IL-1α, IL-6, and IL-8* in HeLa cells treated with **B3C** (0, 5, 10, and 20 μM) for 48 h, and GAPDH was used as the endogenous control (N=3, mean ± SD). (C) The relative proteins expression of SASP related proteins, IL-1α, IL-6, and IL-8 in HeLa cells after the treatments with **B3C** of different concentration (N=3, mean±SD). (D) The cell growth inhibition of **B3C** alone, PI3Ki alone, and **B3C**-PI3Ki combination (10 and 20 μM PI3Ki) to HeLa cells for 48 h, which were measured by MTT assay. (E) Synergy heatmap showing the combination index (CI) for the cells treated **B3C** with PI3Ki at different combinations.

2.6. Combination therapy study for B3C and clinical PI3K inhibitors

To further explore the potential application of **B3C** for further anticancer study, a combination therapy study of **B3C** with different clinical inhibitors of MAPK and PI3K pathways were performed.[28, 68-72] From the MTT results, we found that the MAPK and PI3K inhibitors tested

have IC_{50} values in the range of 18.4-76.8 μM against HeLa cells for 48 h (**Table S6** and **Figure S27**). We then fixed the concentration of inhibitors at 10 and 20 μM and evaluated the inhibitory effects upon combining **B3C** at different concentrations. From the results shown in **Figure 6D**, **Figure S28-S29** and **Table S7**, the **B3C**-PI3Ki combined treatment shows the best inhibitory activity against HeLa cells, as indicated by a markedly reduced IC_{50} values, 1.03 μM (combined with 10 μM PI3Ki) and 0.42 μM (combined with 20 μM PI3Ki), which is much lower than that of the single drug **B3C** (7.6 μM) or PI3Ki (76.8 μM).

To further examine the synergistic or antagonistic effect of **B3C**-PI3Ki combined treatment in HeLa cells, the combination index (CI) of the treatment was analyzed. From **Figure 6E**, the heatmap shows that the CI of different **B3C**-PI3Ki combinations was found lower than 1, which indicates that **B3C**-PI3Ki combined treatment is a synergistic effect. Collectively, these results suggest that combination therapy with **B3C** and clinical inhibitors, such as PI3Ki (GDC0941), may be an effective strategy to treat NRAS-expressing cancers.

3. Discussion

Apart from traditional protein-based targets, the noncanonical secondary structures of nucleic acids such as RNA G-quadruplexes may be potential drug targets of small-molecule ligands. In the present study, we demonstrated that a small-molecule ligand, **B3C** (M^+ = 427 g/mol), was able to interact and image selectively the cellular targets in cytoplasmic region in living HeLa cells, which were proposed to be NRAS mRNA G4s. The ligand showed antiproliferation activity against human HeLa cancer cells (IC_{50} = 7.6 μM), while it exhibited relatively less toxic against noncancerous human fibroblast cells (HFF1: IC_{50} > 50 μM; BJ: IC_{50} > 50 μM). The results of RNA-sequencing showed that the change of cellular RNA in **B3C**-treated HeLa cells was only about 2.4% of the total genes affected, which suggested that the cellular target of **B3C** is highly concentrated. This may imply that the ligand may potentially cause less off-target side effects.

Moreover, it is noteworthy that the downregulation of NRAS by **B3C** in HeLa cells induced DNA damage, which was verified neither a consequence of excessive ROS nor the stress of a direct interaction of **B3C** with the nuclear DNA. Nonetheless, our results suggest that **B3C** may

368 reactivate DDR that is suppressed by NRAS and further induce DNA damage. Further
369 investigations on the DDR also suggest that the treatment of **B3C** may activate both ATR and ATM
370 pathways in HeLa cells. As a result, their downstream effectors, CHK-1 and CHK-2, were
371 phosphorylated. This event may eventually cause the dephosphorylation on CDC25C and
372 phosphorylation on CDK-1, which causes G_2/M cell cycle arresting. The mechanism for the
373 induction of DNA damage by **B3C** is still unclear at present. We speculate that the reactivation of
374 DDR itself may cause replication stress. It has been reported that the activation of DDR may
375 interfere the rapid progression of DNA replication in cancer cells, and cause genomic instability
376 and DNA damage.[73, 74] Moreover, as DNA damage is severe or the repair is insufficient in the
377 cells, the stabilized replication forks following DDR may collapse. This may possibly lead to
378 complex DNA break and thus further enhance DNA damage.[75] Furthermore, the blocking of
379 signaling from PI3K pathway may de-activate or de-stabilize the existing DNA repair protein such
380 as BRCA1 and RAD51.[76] Therefore, the acute DNA damage may happen when NRAS
381 expression is downregulated.

382 Furthermore, our results showed that **B3C** could induce apoptosis in HeLa cells but this was
383 not the only pathway to inhibit HeLa cell proliferation because there were about 30% apoptotic
384 cells found in the assays. The SA-β-gal results indicated that **B3C** could induce senescence, which
385 was supported by the expression of senescence-associated secretory phenotype (SASP) related
386 mRNA and its protein (IL-1α, IL-6 and IL-8). Therefore, **B3C**-induced senescence could be another
387 mechanism to inhibit HeLa cell proliferation.

388 **B3C** was also found a potent ligand in combination therapy against cancers. We examined
389 several clinical inhibitors (targeting MAPK and PI3K pathways) to combine with **B3C** and the
390 results suggested that **B3C**-PI3Ki combination exhibited a much stronger antiproliferation activity
391 against HeLa cells. A markedly reduced IC_{50} value (1.03 μM and 0.42 μM) is achieved, which is
392 notably lower than that of **B3C** (7.6 μM) or PI3Ki (76.8 μM) alone. The combination index (CI)
393 study indicates that the combined treatment is synergism.

394 In conclusion, we developed a cytoplasm-localized ligand (**B3C**) that could possibly target

and image RNA G4-structures, such as NRAS mRNA G4s, in HeLa cells for chemical biology and antiproliferation study. We also demonstrated that **B3C** effectively inhibited HeLa cell proliferation. The downregulation of NRAS protein expression and the induction of apoptosis and senescence were proposed to be the possible antiproliferation mechanisms of **B3C**. To the best of our knowledge, this is the first study that a small-molecule ligand capable of targeting and stabilizing NRAS mRNA G4s could reactivate DNA damage response that is abrogated by NRAS or RAS proteins in cancer cells such as HeLa cells. Our finding may provide new insights into the chemical biology and drug discovery targeting RAS mRNA G4s against RAS-driven cancers.

4. Materials and Methods

All chemical reagents and solvents were analytical reagent grade and were used without further purification. All oligonucleotides and primers used in this work were synthesized and purified by BGI Genomics and their secondary structures were determined by circular dichroism in Tris-HCl buffer prepared using diethyl pyrocarbonate (DEPC)-treated water (ThermoFisher Scientific). All cell lines used in the study were purchased from ATCC.

Synthesis and characterization of ligands (B1C, B2C and **B3C)**

2-Methylbenzothiazole (1 g, 6.7 mmol) and 3-bromopropionic acid (1.13 g, 7.4 mmol) (or 3-bromopropanol or 3-bromopropionamide) were added to a clean pressure vessel and then 5.0 mL acetonitrile was added into the mixture. The vessel was then closed, and the mixture was heated up for reaction under stirring at 110 °C under stirring conditions for 48 h. Reactions were monitored by TLC. After completion, the reaction was cooled to room temperature and 30 mL of ethyl acetate were added to the mixture. The precipitated solid was collected by suction filtration. The solid obtained was dissolved in minimum amount of D.I. H_2O and then was extracted with 15 mL ethyl acetate for 3 times. Intermediate **A** was obtained by removing D.I. H2O under vacuum. To the mixture of intermediate **A** (50 mg, 0.173 μmol) and N-ethylcarbazole-3-carboxaldehyde (44.3 mg, 0.208 μmol) in a clean pressure vessel, 1 mL 1-butanol and 5 mg potassium carbonate were added. The mixture was heated up to 120 °C for reaction under stirring condition for 8 h. The reaction was monitored by TLC. After completion, the reaction mixture was cooled down to room

temperature. The precipitated solid was washed with ethyl acetate and collected under suction filtration. The solids collected were then further purified by column chromatography using a mixture of chloroform and methanol (5:1) as an eluent.

(E)-2-(2-(9-ethyl-9H-carbazol-3-yl)vinyl)-3-(3-hydroxypropyl)benzo[d]thiazol-3-ium bromide (**B1C**). The reddish orange solid was obtained with yield 71%. ^{1}H NMR (400 MHz, DMSO-d_6) δ 8.88 (d, J = 1.7 Hz, 1H), 8.49 – 8.38 (m, 2H), 8.31 – 8.16 (m, 3H), 8.05 (d, J = 15.6 Hz, 1H), 7.90 – 7.81 (m, 2H), 7.81 – 7.70 (m, 2H), 7.57 (ddd, J = 8.3, 7.2, 1.2 Hz, 1H), 7.35 (t, J = 7.5 Hz, 1H), 4.98 (t, J = 7.1 Hz, 3H), 4.54 (q, J = 7.1 Hz, 2H), 3.60 (s, 2H), 2.09 (t, J = 6.4 Hz, 2H), 1.37 (t, J = 7.1 Hz, 3H). ^{13}C NMR (101 MHz, DMSO-d_6) δ 171.92, 150.88, 142.21, 141.29, 140.29, 129.23, 128.04, 127.96, 127.69, 126.85, 125.22, 124.23, 123.93, 122.93, 122.22, 120.78, 120.25, 116.34, 110.10, 110.07, 109.83, 57.41, 46.17, 37.44, 31.44, 13.84. Purity: 95% by HPLC. HRMS (ESI-Quadrupole-TOF) calculated m/z for $C_{26}H_{25}N_2OS^+$: 413.1688; found 413.1689.

(E)-3-(3-amino-3-oxopropyl)-2-(2-(9-ethyl-9H-carbazol-3-yl)vinyl)benzo[d] thiazol-3-ium bromide (**B2C**). The reddish orange solid was obtained with yield 81%. ^{1}H NMR (400 MHz, DMSO-d_6) δ 8.88 (d, J = 1.8 Hz, 1H), 8.47 – 8.37 (m, 2H), 8.22 (dt, J = 8.9, 2.7 Hz, 3H), 8.11 (d, J = 15.6 Hz, 1H), 7.88 – 7.81 (m, 2H), 7.75 (dd, J = 14.6, 7.8 Hz, 2H), 7.62 – 7.53 (m, 2H), 7.35 (t, J = 7.5 Hz, 1H), 7.14 (s, 1H), 5.13 (t, J = 6.7 Hz, 2H), 4.54 (q, J = 7.1 Hz, 2H), 2.83 (t, J = 6.6 Hz, 2H), 1.37 (t, J = 7.1 Hz, 3H). ^{13}C NMR (101 MHz, DMSO-d_6) δ 172.33, 170.85, 150.78, 142.25, 141.15, 140.32, 129.24, 128.01, 127.81, 127.59, 126.89, 125.30, 124.23, 124.06, 122.91, 122.21, 120.63, 120.32, 116.58, 110.30, 110.21, 110.15, 45.06, 33.75, 13.85. Purity: 96% by HPLC. HRMS (ESI-Quadrupole-TOF) calculated m/z for $C_{26}H_{24}N_3OS^+$: 426.1640; found 426.1640.

(E)-3-(2-carboxyethyl)-2-(2-(9-ethyl-9H-carbazol-3-yl)vinyl)benzo[d]thiazol-3-ium bromide (**B3C**). The orange solid was obtained with yield 81%. ^{1}H NMR (400 MHz, DMSO-d_6) δ 12.72 (s, 1H), 8.88 (d, J = 1.7 Hz, 1H), 8.48 – 8.38 (m, 2H), 8.24 (t, J = 8.3 Hz, 3H), 8.09 (d, J = 15.6 Hz, 1H), 7.84 (t, J = 8.3 Hz, 2H), 7.75 (dd, J = 15.3, 8.0 Hz, 2H), 7.57 (t, J = 7.7 Hz, 1H), 7.35 (t, J = 7.5 Hz, 1H), 5.11 (t, J = 7.2 Hz, 2H), 4.54 (q, J = 7.1 Hz, 2H), 3.00 (t, J = 7.1 Hz, 2H), 1.37 (t, J = 7.1 Hz, 3H). ^{13}C NMR (101 MHz, DMSO-d_6) δ 172.65, 171.55, 151.00, 142.25, 141.09, 140.30,

129.26, 127.98, 127.91, 126.87, 125.27, 124.20, 122.89, 122.21, 120.65, 120.31, 116.55, 110.20, 110.15, 110.14, 44.47, 37.45, 32.54, 13.85. Purity: 96% by HPLC. HRMS (ESI-Quadrupole-TOF) calculated m/z for $C_{26}H_{23}N_2O_2S^+$: 427.1480; found 427.1478.

Cell culture

Cell lines of human cervix cancer HeLa (CCL-2), human skin cancer A2058 (CRL-2601), human colon cancer HCT116 (CCL-247), human pancreatic duct cancer PANC-1 (CRL-1469), human fibroblast HFF-1 (SCRC-1041), and human fibroblast BJ (CRL-2522) were purchased from ATCC. The cell lines were cultured in different complete medium as shown below: HCT116 was cultured in RPMI 1640 (Gibco) supplemented with 10% FBS (Gibco) and 1% P/S (Gibco). HeLa, A2058, PANC-1, and HFF-1 were cultured in DMEM supplemented with 10% FBS and 1% P/S. BJ was cultured in MEM (Gibco) supplemented with 10% FBS and 1% P/S. The cells were incubated in incubator at 37 °C with 5% CO2. In all experiments needed for cell collection, the cells were trypsinized by 0.25% trypsin-EDTA (Gibco) and suspended in various medium or buffers for further analysis

Fluorescence titration assay

Fluorescence spectra were recorded with an Agilent G9800AA Cary Eclipse (Type II). The slit width of the colorimetric dish is 1 mm and optical diameter is 10 mm. The emission of **B3C** was acquired by exciting the sample in solution at 470 nm. The emission spectra collection range of **B3C** was 485-750 nm. All oligonucleotides were pre-annealed by heating at 95 °C for 10 min in Tris-HCl buffer (10 mM, pH 7.4) with 60 mM KCl before being used for the titration experiments. The annealed oligonucleotides were then allowed cooling to room temperature and used as the stock solution for further use. In the titration, a certain aliquot of a stock solution of oligonucleotides were added into the solution containing **B3C** at the fixed concentration (2 μM) and the final concentration of oligonucleotides was varied from 0 to 10 μM in the titration series. Then, the mixture was stirred for 1 min to allow achieving equilibrium. The emission of the mixture was measured with the fluorescence spectrometer.

UV-Vis titration assay

UV-Vis spectra were obtained using a BioDrop Duo+ UV-Visible spectrophotometer (Biochrom). The absorption spectra were collected in the range was 350-650 nm for **B3C** and its mixture with the annealed oligonucleotides at different concentration at room temperature. All oligonucleotides were pre-annealed by heating at 95 °C for 10 min in Tris-HCl buffer (10 mM, pH 7.4) with 60 mM KCl before being used for the titration experiments. The annealed oligonucleotides were then allowed cooling to room temperature and used as the stock solution for further use. In the titration, a certain aliquot of a stock solution of oligonucleotides were added into the solution containing **B3C** at the fixed concentration (5 μM) and the final concentration of oligonucleotides was varied from 0 to 15 μM in the titration series. The UV-Vis spectra of the mixtures were measured at room temperature using the Spectrophotometer.

Determination of equilibrium constant (K_{eq})

The fluorescence titration data were obtained from fluorescence titration assay for equilibrium binding constant analysis.[77, 78] Based on the data obtained, [Nucleic acid substrate] was taken as the x-axis, F-F_0/F_0 as the y-axis. The binding constant (K_a) was analyzed according to the independent site model by nonlinear fitting to the equation: $y = 0.5B[A + B + x - \sqrt{(A + B + x)^2 - 4Bx}]$ where F_0 represents the fluorescence intensity of the compound when it exists alone, F represents the fluorescence intensity of the compound after adding nucleic acid, Fmax represents the fluorescence intensity when it is titrated to saturation, K_{eq}= B/(A x [**B3C**], N= B/[**B3C**].

Circular Dichroism (CD) measurements

(A) CD spectra measurements

The CD spectra were performed on a J-1500 circular dichroism spectrophotometer (JASCO). In the experiment, a quartz cuvette with a length of 2 mm was used to record the spectrum in a wavelength range of 220 to 340 nm with a 1 nm bandwidth, a 1 nm step slit and 2 s time constant. Each curve was scanned for 3 times with a scan rate of 50 nm/min. After setting the parameters, 300 μL of nucleic acids with a concentration of 5 μM was placed in a colorimetric dish. The CD spectra of the nucleic acid alone were collected first. Then, the CD spectra of the nucleic acid

solutions mixed with **B3C** at different concentrations (10 μM and 25 μM) were collected.

(B) CD melting point assay

CD melting point assays were performed on a J-1500 circular dichroism spectrophotometer (JASCO) and set at a fixed wavelength. In the experiment, a quartz cuvette with a length of 2 mm was used to record the spectrum in the temperature range of 25 to 95 °C with a gradient temperature of 2 °C/min, 1 nm bandwidth, 1 nm step slit, and 2 s time constant. The CD melting spectra of the nucleic acid (10 mM Tris-HCl buffer, pH 7.4 with 20 mM KCl) alone were collected first. Then, the CD melting spectra of the nucleic acid solutions mixed with **B3C** (25 μM) were collected. The melting temperature (T_m) was defined by the temperature when half of ellipticity was gone. The different in melting temperature (ΔT_m) of nucleic acid mixed with or without **B3C** was defined by the different of their own melting temperature.

Cell growth inhibition Analysis

Cell lines were seeded at a density of 3 x 10^3 cells/well in a 96-well plate (TPP). After overnight incubation, the cells were treated with various concentrations of **B3C** for 48 h. After the treatment, the cell viability of different cell lines was determined by MTT assay (ThermoFisher Scientific). Briefly, to the cells treated with ligands, 10 μL of 5 mg/mL MTT was added to each well. The cells were incubated in an incubator at 37 °C with 5% CO_2 for 3 hours. After incubation, the medium was replaced with 100 μL of DMSO (ThermoFisher Scientific). The samples were then subjected to Varioskan LUX Multimode Microplate Reader (ThermoFisher Scientific) and the optical density (OD) of the plates was measured at 540 nm.

Confocal microscopy

(A) Live cell imaging of ligands

HeLa cells were seeded on a 15 mm glass bottom culture dish (NEST Biotechnology) at a density of 10 x 10^4 cells/dish. After incubated for overnight, the cells were first stained with 5 μM **B3C** for 15 mins. The cells were washed with DMEM and then were treated with 2 μM Hoechst 33342 (ThermoFisher Scientific) for 10 min. After washing with medium for three times, the dishes were subjected to TCS SPE confocal microscope (Leica) for confocal imaging. Briefly, Hoechst 33342

and **B3C** were excited at 405 nm and 488 nm with lasers respectively. The emitted signals were recorded sequentially with a photomultiplier tubes (PMT) detector.

(B) MitoTracker co-staining imaging

HeLa cells were seeded on a 15 mm glass bottom culture dish at a density of 10 x 10^4 cells/dish. After overnight incubation, the cells were first stained with 30 nM MitoTracker™ Deep Red (ThermoFisher Scientific) for 30 mins. Then, the cells were washed with DMEM for three times and were treat with 5 μM **B3C** by following the procedures described above in **(A)**.

(C) RNase and DNase digestion assay

HeLa cells were seeded on a 15 mm glass bottom culture dish (NEST Biotechnology) at a density of 10 x 10^4 cells/dish. After overnight incubation, the cells were first washed with DMEM for three time. To the washed cells, it was first stained with 5 μM **B3C** for 15 mins. And then the cells were washed with PBS for three times and fixed with 4% paraformaldehyde for 30 mins at room temperature. The cells after being fixed were washed with PBS for another three times to remove the paraformaldehyde and treated with 0.5% triton X-100 for 1 h. After washed with PBS for three times, the fixed cells were treated with 200 units/mL RNase or DNase in buffer provided. The cells were then incubated at 37 °C for 2 hours. After enzyme digestion, the fixed cells were washed with PBS for three times. Then, the cells were stained with 2 μM DAPI (ThermoFisher Scientific) at room temperature for 10 mins. After washing with PBS for three times, the dishes were subjected to TCS SPE confocal microscope (Leica) for confocal imaging. Briefly, DAPI and **B3C** were excited at 405 nm and 488 nm with lasers respectively. The emitted signals were recorded sequentially with a PMT detector.

(D) Immunofluorescence staining assay

HeLa cells were seeded on a 15 mm glass bottom culture dish (NEST Biotechnology) at a density of 50 x 10^4 cells/dish. After overnight incubation, the cells were first washed with DMEM for three time. To the washed cells, it was first live stained with 5 μM **B3C** for 15 mins (BG4, LAMP-1) or 48h (Ki-67). And then the cells were washed with PBS for three times and fixed with 4% paraformaldehyde for 30 mins at room temperature. Subsequently, the cells were permeabilized

by incubating in 0.5% Triton-X containing PBS for 1 hour in room temperature. After washing with PBS for three times, the cells were further blocked with 1% BSA (in PBS). After that, the cells were directly incubated with antibody (BG4, 1:750 in PBS containing 1% BSA; Ki67, Beyotime, 1:1000 in PBS containing 1% BSA; LAMP1,ThermoFisher Scientific, 1:1000 in PBS containing 1% BSA) at 4 °C. After overnight incubation, the cells were first washed with ice-cooled PBS for 5 times and were incubated with goat anti-rabbit IgG Alexa Fluor 647 (ThermoFisher Scientific) or goat anti-mouse IgG Alexa Fluor 647 (ThermoFisher Scientific) in 1:1000 dilution (PBS containing 1%BSA) for another 1.5 hours. After secondary antibody incubation, the cells were washed with ice-cold PBS for 3 times. Then, the cells were stained with 2 μM DAPI at room temperature for 10 mins. After washing with PBS for three times, the dishes were subjected to TCS SPE confocal microscope (Leica) for confocal imaging. Briefly, DAPI, **B3C**, and Alexa Fluor 647 were excited at 405 nm, 488 nm, and 635 nm with lasers respectively. The emitted signals were recorded sequentially with a PMT detector.

Quantitative Real-time PCR (qRT-PCR)

HeLa cells were seeded on a 10 cm culture dish. After overnight incubation, the cells were treated with **B3C** at different concentration for 48 h. After treatment, the cells were trypsinized and subjected to RNA extraction with RNeasy Mini kit (Qiagen). The RNA samples were prepared according to the manufacturer's instructions. After quantifying the concentration by BioDrop Duo+ UV-Vis spectrophotometer (Biochrom), the RNA samples were diluted to 0.05 μg/μL. The qRT-PCR mixtures were done with BeyoFast™ SYBR Green One-Step qRT-PCR Kit (Beyotime) according to the manufacturer's instructions in which 2 μL 0.05 μg/μL RNA solution, 2 μL of 3 uM forward and reverse primer mixture solution, and low ROX were used in each PCR reaction. The RNA mixtures were then subjected to QuantStudio™ 5 Real-time PCR system (Applied Biosystems). The conditions of qRT-PCR were listed as follows: one cycle of 50 °C for 30 mins, followed by one cycle of 90 °C for 2 mins, followed with 40 cycles of 95 °C for 15 seconds, 60 °C for 30 seconds, and 72 °C for 30 seconds. All experiments were run in triplicate and the gene expression level was normalized with housekeeping gene GAPDH.

Western blotting

HeLa cells were seeded on a 6 cm culture dish. After overnight incubation, the cells were treated with **B3C** at different concentration for 48 h. After treatment, the cells were trypsinized and lyzed in 4 °C in RIPA buffer (50 mM HCl, 150 mM NaCl, 1% NP-40, 0.5% sodium deoxycholate and 0.1% SDS, pH 7.4) supplemented with protease and phosphatase inhibitors (CST). Total protein concentration was determined by Detergent Compatible Bradford Protein Assay Kit (Beyotime) according to the manufacturer's instructions. Equal concentration of proteins was mixed with 4x Laemmli sample buffer (Biorad) then subjected to a heat plate for denaturing at 95 °C for 10 mins. Then, the proteins were loaded onto 8 or 10 or 12% SDS-PAGE gel for electrophoresis. The gels were then transferred onto PVDF membrane (Milipore) by electroblotting. Membranes were blocked with 5% skim milk (Beyotime) for 2 h. After blocking, membranes were incubated with the primary antibody at 4 °C overnight. Primary antibodies used were listed as follow: TRF2 (Abcam, ab108997), NRAS (Abcam, ab300431), KRAS (Abcam, ab275885), VEGFA (Abcam, ab214424), gamma H2A.X (Ser139) (Abcam, ab22551), p53 (ThermoFisher Scientific, MA5-14516), p-p53 (Ser15) (ThermoFisher Scientific, MA5-15229), PARP-1 (CST, 9532), Caspase-3 (CST, 9662), cleaved Caspase-3 (CST, 9664), ATR (CST, 13934), p-ATR (Ser428) (ThermoFisher Scientific, 720107), CHK-1 (ThermoFisher Scientific, MA5-32180), p-CHK-1 (Ser345) (MA5-165145), ATM (CST, 2873), p-ATM (Ser1981) (CST, 13050), CHK-2 (CST, 2662), p-CHK-2 (Thr68) (CST, 2661), CDC25C (ThermoFisher Scientific, MA5-33127), p-CDC25C (Ser216) (ThermoFisher Scientific, MA5-15146), CDK-1 (ThermoFisher Scientific, 33-1800), p-CDK1 (ThermoFisher Scientific, 44-686G), GAPDH (ThermoFisher Scientific, MA5-15738) and beta-Actin (CST, 3700). The concentrations of primary antibodies were prepared based on the recommendation of the manufacturer. After incubation and repeated washing with TBST at room temperature for 5 mins four times, membranes were incubated with Goat anti-Rabbit IgG (H+L), horseradish peroxidase (HRP)-conjugated secondary antibody (ThermoFisher Scientific #65-6120) or Goat anti-Mouse IgG (H+L), horseradish peroxidase (HRP)-conjugated secondary antibody (ThermoFisher Scientific #62-6520) for 2 hours. After incubation, membranes were extensively washed with TBST

for three times and subjected to chemiluminescence detection using SuperSignal™ West Atto Ultimate Sensitivity Substrate (ThermoFisher Scientific) according to the manufacturer's instructions under ChemiDoc MP Integrated Imaging System (Bio-rad).

Dual-Luciferase assay

The psiCHECK2 vector was purchased from Promega. The insert sequences (WT and Mut) were generated and cloned by Genscript. Specifically, the insert sequences were ligated right before NheI site. HeLa cells were seeded on a black 96 well plate at a density of 15000 cells/well. After overnight incubation, the plasmids (100ng/well) were transfected into HeLa cells using Lipofectamine 3000 (Invitrogen) according to the manufacturer's instructions. After 4 h, different concentration of **B3C** in medium was directly added to the cells without removing the original medium to give a final concentration of **B3C** of 0, 5, 10, and 20 uM. The samples were incubated at 37 °C with CO_2 for another 24 h. Dual-luciferase assays were subsequently performed using Dual-Glo® Luciferase Assay System according to the manufacturer's instructions. The quantification was performed using a multimode microplate reader (BMG LABTECH CLARIOstar). The secreted *Renilla* activity was normalized to the Firefly luciferase activity. All of the experiments were repeated three times.

RNA Immunoprecipitation (RIP)

HeLa cells were seeded on a 15 cm culture dish. After incubation to 70% confluency, the cells were treated with or without 20 uM **B3C** at 37 °C with CO_2 for 48 h. The RIP was subsequently performed using Magna RIP™ RNA-Binding Protein Immunoprecipitation Kit (Millipore) according to the manufacturer's instructions. The obtained RNA was used for qRT-PCR detection using BeyoFast™ SYBR Green One-Step qRT-PCR Kit (Beyotime).

RNA sequencing

HeLa cells were seeded in a 10 cm culture flask (TPP). After overnight incubation, the cells were treated with 20 μM **B3C** for 48 h. After treatment, the cells were trypsinized and subjected to RNA extraction with RNeasy Mini kit (Qiagen). The RNA samples were prepared according to the manufacturer's instructions. After that, the RNA samples were sent to Novogene company for RNA

sequencing and data analysis. The raw transcriptome data have been deposited in NCBI Sequence Read Archive (SRA) database (**BioProject: PRJNA1123410**). Briefly, the quantity and quality of RNA samples were assessed by Qubit 4.0 fluorometer (ThermoFisher Scientific) and Agilent 2100 Bioanalyzer (Agilent) respectively. cDNA libraries were prepared from RNA samples with Illumina TruSeq Stranded Total RNA Prep kit (ligation with Ribo-Zero Plus) and indexing kit (Illumina). The quantity and quality of the prepared cDNA libraries were assessed by Qubit 4.0 fluorometer and Agilent 2100 Bioanalyzer, respectively. The cDNA libraries of experimental and control groups were pooled, and the sequencing was done by an Illumina NextSeq 2000 system with the 150bp paired-end dual-indexed method. The sequencing quality of the experimental and control samples was determined by FastQC. The low-quality reads and adapter sequences were trimmed with Fastp. The trimmed reads were further aligned to the human reference genome (GRCh38/hg38) with STAR package (R programming). The STAR output (reads per gene) was subjected to DESeq2 (R programming) to perform differential expression analysis. Genes with fold-change >1 or < −1 and p-value <0.05 were defined as differentially expressed genes. By this criterion, a heat map of expression patterns was generated in R (pheatmap). The volcano plot was drawn with R (ggplot2). Kyoto Encyclopedia of Genes and Genomes (KEGG) analysis was performed with clusterprofiler (R programming). Gene Set Enrichment Analysis (GSEA) was carried out using the GSEA software 4.1.0 (Broad Institute) with hallmark gene sets (H collection) and canonical pathways gene sets (CP in C2 collection) in Molecular Signatures Database (MSigDB 7.2).

Comet assay

The DNA damage in HeLa cells was detected by the Comet assay kit (Abcam, ab238544). After overnight incubation, the cells were treated with different concentrations of **B3C** for 48 h. After treatment, the cells were collected by trypsinization with 0.25% trypsin with EDTA and suspended in ice-cold PBS at 1×10^5 cells/mL. The sample was prepared according to the manufacturer's instruction. Briefly, cells were mixed with comet agarose at 37 °C and the agarose/cell mixture was pipetted onto the top of the base layer of comet agarose. The slide was transferred to 4 °C in

666 the dark for 15 min for gelation. The slide was then transferred to a container with prechilled lysis
667 buffer for 30 min at 4 °C in the dark. After lysis buffer treatment, the slide was treated with alkaline
668 solution for 30 min at 4 °C in the dark. The treated slide was then transferred to a horizontal
669 electrophoresis chamber for electrophoresis under an alkaline electrophoresis solution (300 mM
670 NaOH and 1 mM EDTA, pH > 13), with 30 V for 30 min. The slide was washed twice with cold
671 water and immersed in cold 70% ethanol for 5 min. The slide was then allowed to air-dry and was
672 treated with 2 μM DAPI for 10 min. The slide was subjected to The Zeiss AxioVert A1 Inverted
673 Microscope for imaging.

674 **Colony formation assay**

675 HeLa cells were seeded at a density of 500 cells/well in a 6-wells plate. After overnight incubation,
676 the cells were treated with the **B3C** at different concentrations for 10 days. The samples were then
677 treated with crystal violet (Beyotime Biotechnology) for 30 min. After washing with PBS for 3 times,
678 the plates were dried and subjected to The Olympus CKX53 inverted microscope for imaging.

679 **Wound healing assay**

680 HeLa cells were seeded in a 6-wells plate. After reaching 90% confluence, the HeLa cells were
681 wounded with a p20 pipette tip. The cells were then washed with PBS for 3 times and incubated
682 with treated with or without 20 uM **B3C** at 37 °C with CO_2 for 48 h. After washing with PBS for 3
683 times, the plates were subjected to The Olympus CKX53 inverted microscope for imaging.

684 **Flow cytometry**

685 **(A) Apoptosis analysis**

686 HeLa cells were seeded on a 6-well plate. After overnight incubation, the cells were treated with
687 different concentration of **B3C** at 37 °C with CO_2 for 48 h. The cells were collected by trypsinization
688 with 0.25% trypsin with EDTA. The collected cells were resuspended in binding buffer using
689 BUV396 conjugated Annexin V (BD Biosciences) and 7-AAD (BD Biosciences) according to the
690 manufacturer's instruction. The stained cells were subjected to A3 Cell Analyzer (BD
691 FACSymphony) for apoptotic analysis.

692 **(B) Cell cycle analysis**

The cell cycle analysis was performed by Cell Cycle and Apoptosis Analysis Kit (Beyotime). HeLa cells were seeded at a density of 20 x 10^4 cells/well in a 6-wells plate. After overnight incubation, the cells were treated with **B3C** at different concentration for 24 hours. After the treatment, the cells were collected by trypsinization with 0.25% trypsin with EDTA and suspended in ice-cooled PBS. After centrifugation at 1200 rpm for 5 mins to remove the supernatant, 1mL ice-cooled 70% Ethanol (in PBS) were added, mixed well, and incubated at 4 °C for 2 hours. After fixation, the cells were centrifuged at 3000 rpm for 5 min to remove supernatant. The cells were then stained with propidium iodide (PI) according to the manufacturer's instructions. The stained cells were subjected to flow cytometry (BD Accuri C6 flow cytometer) for cell cycle analysis.

β-Galactosidase (SA-β-gal) staining of cell senescence

HeLa cells were seeded at a density of 1 x 10^4 cells/well in a 6-wells plate. After overnight incubation, the cells were treated with the **B3C** at different concentrations. Then, the HeLa cells were incubated for 7 days. After incubation, the medium was discarded, and the cells were washed with PBS for 3 times. The cells were then performed the SA-β-gal staining with Senescence β-Galactosidase Staining Kit (Beyotime) according to the manufacturer's instructions. After staining, the cells were first rinsed with 70% ethanol (in PBS) followed by two PBS washing. The cells were then subjected to Primovert Inverted Microscope (Zeiss) for imaging.

Enzyme-Linked Immunosorbent Assay (ELISA)

HeLa cells were seeded on a 6 cm culture dish. After overnight incubation, the cells were treated with B3C at different concentration for 48 h. After treatment, the cells were trypsinized and lyzed in 4 °C in RIPA buffer (50 mM HCl, 150 mM NaCl, 1% NP-40, 0.5% sodium deoxycholate and 0.1% SDS, pH 7.4) supplemented with protease and phosphatase inhibitors (CST). Total protein concentration was determined by Detergent Compatible Bradford Protein Assay Kit (Beyotime) according to the manufacturer's instructions. Equal concentration of proteins was used in assay kit and performed according to the manufacturer's instructions. ELISA kits used were listed as follow: Human IL-1 alpha ELISA Kit (Abcam, AB100560-96T), Human IL-6 ELISA kit (Abcam, AB178013-96T), and Human IL-8 ELISA kit (Abcam, 214030-96T). The samples were then

subjected to Varioskan LUX Multimode Microplate Reader (ThermoFisher Scientific) and the optical density (OD) of the plates was measured at 600 nm.

Statistical test

Statistical analysis was done by one-way ANOVA with Tukey as statistical hypothesis test using GraphPad Prism. All bioassays were repeated at least three times ($N \geq 3$, mean ± S.D.); (*) $P < 0.05$, (**) $P < 0.01$ and (***) $P < 0.001$, significantly different from each data set; ns, not significantly different from each data set.

Data availability statement

The data supporting this article have been included as part of the Supplementary Information. The raw transcriptome data were deposited in NCBI Sequence Read Archive (SRA) database, BioProject: PRJNA1123410.

Acknowledgments

The work described in this paper was supported by the grants from the Research Grants Council of the Hong Kong Special Administrative Region, China (RGC Project No. 15300522) and the Health and Medical Research Fund, Hong Kong SAR (Project No. 19200231). The University Research Facilities on Life Sciences and Chemical and Environmental Analysis of The Hong Kong Polytechnic University are also acknowledged.

Author contribution

K.-H.C. carried out the experiments, analyzed the data, and mainly wrote the manuscript. B.-X.Z., A.S.-L.L., W.L., Y.C., and Y.Z. assisted in conducting the study. B.-X.Z., A.S.-L.L., and W.L. analyzed the data and organized figures. W.-L.W. conceived the project idea, supervised the work, and revised the manuscript.

Declaration of interest

Authors declare that they do not have any financial or commercial interest regarding this article.

Keywords: NRAS mRNA G-quadruplex structure; mRNA G4-targeting ligand; DNA damage response; Combination therapy; Antiproliferation

Reference:

[1] C.J. Der, D. Vigil, J. Cherfils, K.L. Rossman, Ras superfamily GEFs and GAPs: validated and tractable targets for cancer therapy?, Nature reviews. Cancer 10(12) (2010) 842-857.

[2] E. Grabocka, Y. Pylayeva-Gupta, Mathew J.K. Jones, V. Lubkov, E. Yemanaberhan, L. Taylor, Hao H. Jeng, D. Bar-Sagi, Wild-Type H- and N-Ras Promote Mutant K-Ras-Driven Tumorigenesis by Modulating the DNA Damage Response, Cancer cell 25(2) (2014) 243-256.

[3] M.F. Olson, R. Marais, Ras protein signalling, Seminars in Immunology 12(1) (2000) 63-73.

[4] D.K. Simanshu, D.V. Nissley, F. McCormick, RAS Proteins and Their Regulators in Human Disease, Cell 170(1) (2017) 17-33.

[5] F.C. Kelleher, G.A. McArthur, Targeting NRAS in melanoma, The cancer journal (Sudbury, Mass.) 18(2) (2012) 132-136.

[6] P. Rodriguez-Viciana, C. Sabatier, F. McCormick, Signaling Specificity by Ras Family GTPases Is Determined by the Full Spectrum of Effectors They Regulate, Molecular and Cellular Biology 24(11) (2004) 4943-4954.

[7] M. Malumbres, M. Barbacid, RAS oncogenes: the first 30 years, Nature reviews. Cancer 3(6) (2003) 459-465.

[8] I. Wortzel, R. Seger, The ERK cascade: Distinct functions within various subcellular organelles, Genes & cancer 2(3) (2011) 195-209.

[9] M. Drosten, A. Dhawahir, E.Y.M. Sum, J. Urosevic, C.G. Lechuga, L.M. Esteban, E. Castellano, C. Guerra, E. Santos, M. Barbacid, Genetic analysis of Ras signalling pathways in cell proliferation, migration and survival, The EMBO Journal 29(6) (2010) 1091-1104-1104.

[10] M. Eskandarpour, F. Huang, K.A. Reeves, E. Clark, J. Hansson, Oncogenic NRAS has multiple effects on the malignant phenotype of human melanoma cells cultured in vitro, Int J Cancer 124(1) (2009) 16-26.

[11] J. Canon, K. Rex, A.Y. Saiki, C. Mohr, K. Cooke, D. Bagal, K. Gaida, T. Holt, C.G. Knutson, N. Koppada, B.A. Lanman, J. Werner, A.S. Rapaport, T. San Miguel, R. Ortiz, T. Osgood, J.-R. Sun, X. Zhu, J.D. McCarter, L.P. Volak, B.E. Houk, M.G. Fakih, B.H. O'Neil, T.J. Price, G.S. Falchook, J. Desai, J. Kuo, R. Govindan, D.S. Hong, W. Ouyang, H. Henary, T. Arvedson, V.J. Cee, J.R. Lipford, The clinical KRAS(G12C) inhibitor AMG 510 drives anti-tumour immunity, Nature (London) 575(7781) (2019) 217-223.

[12] J.B. Fell, J.P. Fischer, B.R. Baer, J.F. Blake, K. Bouhana, D.M. Briere, K.D. Brown, L.E. Burgess, A.C. Burns, M.R. Burkard, H. Chiang, M.J. Chicarelli, A.W. Cook, J.J. Gaudino, J. Hallin, L. Hanson, D.P. Hartley, E.J. Hicken, G.P. Hingorani, R.J. Hinklin, M.J. Mejia, P. Olson, J.N. Otten, S.P. Rhodes, M.E. Rodriguez, P. Savechenkov, D.J. Smith, N. Sudhakar, F.X. Sullivan, T.P. Tang, G.P. Vigers, L. Wollenberg, J.G. Christensen, M.A. Marx, Identification of the Clinical Development Candidate MRTX849, a Covalent KRASG12C Inhibitor for the Treatment of Cancer, Journal of Medicinal Chemistry 63(13) (2020) 6679-6693.

[13] Z.R.T. Sumirtha Balaratnam, David R. Calabrese, Michael T. Banco, Kamyar Yazdani,, A.R.F.-D.A. Xiao Liang, Danny Incarnato, and John S. Schneekloth Jr, Investigating the NRAS 5' UTR as a Target for Small Molecules, Obesity, fitness, & wellness week (2022) 1031.

[14] A. Boespflug, J. Caramel, S. Dalle, L. Thomas, Treatment of NRAS-mutated advanced or

metastatic melanoma: rationale, current trials and evidence to date, Ther Adv Med Oncol 9(7) (2017) 481-492.
[15] J.R. Remsberg, R.M. Suciu, N.A. Zambetti, T.W. Hanigan, A.J. Firestone, A. Inguva, A. Long, N. Ngo, K.M. Lum, C.L. Henry, S.K. Richardson, M. Predovic, B. Huang, M.M. Dix, A.R. Howell, M.J. Niphakis, K. Shannon, B.F. Cravatt, ABHD17 regulation of plasma membrane palmitoylation and N-Ras-dependent cancer growth, Nature chemical biology 17(8) (2021) 856-864.
[16] T. Randic, I. Kozar, C. Margue, J. Utikal, S. Kreis, NRAS mutant melanoma: Towards better therapies, Cancer treatment reviews 99 (2021) 102238-102238.
[17] M. Mandalà, B. Merelli, D. Massi, Nras in melanoma: Targeting the undruggable target, Critical reviews in oncology/hematology 92(2) (2014) 107-122.
[18] S. Burge, G.N. Parkinson, P. Hazel, A.K. Todd, S. Neidle, Quadruplex DNA: sequence, topology and structure, Nucleic acids research 34(19) (2006) 5402-5415.
[19] E.A. Venczel, D. Sen, Parallel and antiparallel G-DNA structures from a complex telomeric sequence, Biochemistry (Easton) 32(24) (1993) 6220-6228.
[20] D. Gomez, T. Lemarteleur, L. Lacroix, P. Mailliet, J.L. Mergny, J.F.o. Riou, Telomerase downregulation induced by the G-quadruplex ligand 12459 in A549 cells is mediated by hTERT RNA alternative splicing, Nucleic acids research 32(1) (2004) 371-379.
[21] S. Kumari, J.L. Huppert, S. Balasubramanian, A. Bugaut, An RNA G-quadruplex in the 5′ UTR of the NRAS proto-oncogene modulates translation, Nature chemical biology 3(4) (2007) 218-221.
[22] J.-D. Beaudoin, J.-P. Perreault, Exploring mRNA 3′-UTR G-quadruplexes: Evidence of roles in both alternative polyadenylation and mRNA shortening, Nucleic acids research 41(11) (2013) 5898-5911.
[23] A.C. Blice-Baum, M.-R. Mihailescu, Biophysical characterization of G-quadruplex forming FMR1 mRNA and of its interactions with different fragile X mental retardation protein isoforms, RNA (Cambridge) 20(1) (2014) 103-114.
[24] S. Kumari, A. Bugaut, S. Balasubramanian, Position and Stability Are Determining Factors for Translation Repression by an RNA G-Quadruplex-Forming Sequence within the 5′ UTR of the NRAS Proto-oncogene, Biochemistry (Easton) 47(48) (2008) 12664-12669.
[25] W. Peng, Z.Y. Sun, Q. Zhang, S.Q. Cheng, S.K. Wang, X.N. Wang, G.T. Kuang, X.X. Su, J.H. Tan, Z.S. Huang, T.M. Ou, Design, Synthesis, and Evaluation of Novel p-(Methylthio)styryl Substituted Quindoline Derivatives as Neuroblastoma RAS (NRAS) Repressors via Specific Stabilizing the RNA G-Quadruplex, J Med Chem 61(15) (2018) 6629-6646.
[26] X.-C. Chen, G.-X. Tang, J. Dai, L.-T. Dai, T.-Y. Wu, W.-W. Li, T.-M. Ou, Z.-S. Huang, J.-H. Tan, S.-B. Chen, Discovery of Clinically Used Octenidine as NRAS Repressor That Effectively Inhibits NRAS-Mutant Melanoma, Journal of medicinal chemistry 66(7) (2023) 5171-5184.
[27] B. Herdy, C. Mayer, D. Varshney, G. Marsico, P. Murat, C. Taylor, C. D'Santos, D. Tannahill, S. Balasubramanian, Analysis of NRAS RNA G-quadruplex binding proteins reveals DDX3X as a novel interactor of cellular G-quadruplex containing transcripts, Nucleic acids research 46(21) (2018) 11592-11604.
[28] D. Sarker, J.E. Ang, R. Baird, R. Kristeleit, K. Shah, V. Moreno, P.A. Clarke, F.I. Raynaud, G. Levy, J.A. Ware, K. Mazina, R. Lin, J. Wu, J. Fredrickson, J.M. Spoerke, M.R. Lackner, Y. Yan, L.S. Friedman,

S.B. Kaye, M.K. Derynck, P. Workman, J.S. De Bono, First-in-human phase I study of pictilisib (GDC-0941), a potent pan-class I phosphatidylinositol-3-kinase (PI3K) Inhibitor, in patients with advanced solid tumors, Clinical cancer research 21(1) (2015) 77-86.
[29] A.W. Schmidt, K.R. Reddy, H.-J. Knölker, Occurrence, Biogenesis, and Synthesis of Biologically Active Carbazole Alkaloids, Chemical reviews 112(6) (2012) 3193-3328.
[30] W.-C. Huang, T.-Y. Tseng, Y.-T. Chen, C.-C. Chang, Z.-F. Wang, C.-L. Wang, T.-N. Hsu, P.-T. Li, C.-T. Chen, J.-J. Lin, P.-J. Lou, T.-C. Chang, Direct evidence of mitochondrial G-quadruplex DNA by using fluorescent anti-cancer agents, Nucleic acids research 43(21) (2015) 10102-10113.
[31] M.-H. Hu, Y.-Q. Wang, Z.-Y. Yu, L.-N. Hu, T.-M. Ou, S.-B. Chen, Z.-S. Huang, J.-H. Tan, Discovery of a New Four-Leaf Clover-Like Ligand as a Potent c-MYC Transcription Inhibitor Specifically Targeting the Promoter G-Quadruplex, Journal of medicinal chemistry 61(6) (2018) 2447-2459.
[32] T.-Y. Wu, X.-C. Chen, G.-X. Tang, W. Shao, Z.-C. Li, S.-B. Chen, Z.-S. Huang, J.-H. Tan, Development and Characterization of Benzoselenazole Derivatives as Potent and Selective c-MYC Transcription Inhibitors, Journal of medicinal chemistry 66(8) (2023) 5484-5499.
[33] M. Di Antonio, G. Biffi, A. Mariani, E.-A. Raiber, R. Rodriguez, S. Balasubramanian, Selective RNA Versus DNA G-Quadruplex Targeting by In Situ Click Chemistry, Angewandte Chemie 124(44) (2012) 11235-11240.
[34] G. Biffi, M. Di Antonio, D. Tannahill, S. Balasubramanian, Visualization and selective chemical targeting of RNA G-quadruplex structures in the cytoplasm of human cells, Nat Chem 6(1) (2014) 75-80.
[35] R. Rodriguez, S. Müller, J.A. Yeoman, C. Trentesaux, J.-F. Riou, S. Balasubramanian, A Novel Small Molecule That Alters Shelterin Integrity and Triggers a DNA-Damage Response at Telomeres, Journal of the American Chemical Society 130(47) (2008) 15758-15759.
[36] A. Bugaut, R. Rodriguez, S. Kumari, S.T. Hsu, S. Balasubramanian, Small molecule-mediated inhibition of translation by targeting a native RNA G-quadruplex, Org Biomol Chem 8(12) (2010) 2771-6.
[37] L.-Y. Liu, T.-Z. Ma, Y.-L. Zeng, W. Liu, Z.-W. Mao, Structural Basis of Pyridostatin and Its Derivatives Specifically Binding to G-Quadruplexes, Journal of the American Chemical Society 144(26) (2022) 11878-11887.
[38] A.M. Burger, F. Dai, C.M. Schultes, A.P. Reszka, M.J. Moore, J.A. Double, S. Neidle, The G-quadruplex-interactive molecule BRACO-19 inhibits tumor growth, consistent with telomere targeting and interference with telomerase function, Cancer research (Chicago, Ill.) 65(4) (2005) 1489-1496.
[39] B.-X. Zheng, W. Long, M.-T. She, Y. Wang, D. Zhao, J. Yu, A. Siu-Lun Leung, K. Hin Chan, J. Hou, Y.-J. Lu, W.-L. Wong, A Cytoplasm-Specific Fluorescent Ligand for Selective Imaging of RNA G-Quadruplexes in Live Cancer Cells, Chemistry : a European journal (2023) e202300705-e202300705.
[40] Z. Deng, J. Norseen, A. Wiedmer, H. Riethman, P.M. Lieberman, TERRA RNA Binding to TRF2 Facilitates Heterochromatin Formation and ORC Recruitment at Telomeres, Molecular cell 35(4) (2009) 403-413.
[41] Y. Mei, Z. Deng, O. Vladimirova, N. Gulve, F.B. Johnson, W.C. Drosopoulos, C.L. Schildkraut,

P.M. Lieberman, TERRA G-quadruplex RNA interaction with TRF2 GAR domain is required for telomere integrity, Sci Rep 11(1) (2021) 3509.
[42] W. Klapper, W. Qian, C. Schulte, R. Parwaresch, DNA damage transiently increases TRF2 mRNA expression and telomerase activity, Leukemia 17(10) (2003) 2007-2015.
[43] A. Arora, M. Dutkiewicz, V. Scaria, M. Hariharan, S. Maiti, J. Kurreck, Inhibition of translation in living eukaryotic cells by an RNA G-quadruplex motif, RNA (Cambridge) 14(7) (2008) 1290-1296.
[44] P. Agarwala, S. Pandey, S. Maiti, Role of G-quadruplex located at 5′ end of mRNAs, Biochimica et Biophysica Acta (BBA) - General Subjects 1840(12) (2014) 3503-3510.
[45] E.P. Booy, M. Meier, N. Okun, S.K. Novakowski, S. Xiong, J. Stetefeld, S.A. McKenna, The RNA helicase RHAU (DHX36) unwinds a G4-quadruplex in human telomerase RNA and promotes the formation of the P1 helix template boundary, Nucleic Acids Research 40(9) (2012) 4110-4124.
[46] L.J. Mah, A. El-Osta, T.C. Karagiannis, γH2AX: a sensitive molecular marker of DNA damage and repair, Leukemia 24(4) (2010) 679-686.
[47] M. Podhorecka, A. Skladanowski, P. Bozko, H2AX Phosphorylation: Its Role in DNA Damage Response and Cancer Therapy, Journal of nucleic acids 2010 (2010) 1-9.
[48] Y.S. Bae, H. Oh, S.G. Rhee, Y.D. Yoo, Regulation of Reactive Oxygen Species Generation in Cell Signaling, Molecules and Cells 32(6) (2011) 491-509.
[49] B.-X. Zheng, W. Long, W. Zheng, Y. Zeng, X.-C. Guo, K.-H. Chan, M.-T. She, A.S.-L. Leung, Y.-J. Lu, W.-L. Wong, Mitochondria-Selective Dicationic Small-Molecule Ligand Targeting G-Quadruplex Structures for Human Colorectal Cancer Therapy, Journal of Medicinal Chemistry 67(8) (2024) 6292-6312.
[50] A. Abulaiti, A.J. Fikaris, O.M. Tsygankova, J.L. Meinkoth, Ras induces chromosome instability and abrogation of the DNA damage response, Cancer research (Chicago, Ill.) 66(21) (2006) 10505-10512.
[51] D.W. Meek, Tumour suppression by p53: a role for the DNA damage response?, Nature Reviews Cancer 9(10) (2009) 714-723.
[52] A. Hirao, Y.-Y. Kong, S. Matsuoka, A. Wakeham, J. Ruland, H. Yoshida, D. Liu, S.J. Elledge, T.W. Mak, DNA Damage-Induced Activation of p53 by the Checkpoint Kinase Chk2, Science (American Association for the Advancement of Science) 287(5459) (2000) 1824-1827.
[53] A.N. Blackford, S.P. Jackson, ATM, ATR, and DNA-PK: The Trinity at the Heart of the DNA Damage Response, Molecular Cell 66(6) (2017) 801-817.
[54] A. Maréchal, L. Zou, DNA damage sensing by the ATM and ATR kinases, Cold Spring Harbor perspectives in biology 5(9) (2013) a012716-a012716.
[55] M. Thanasoula, J.M. Escandell, N. Suwaki, M. Tarsounas, ATM/ATR checkpoint activation downregulates CDC25C to prevent mitotic entry with uncapped telomeres, The EMBO Journal 31(16) (2012) 3398-3410-3410.
[56] A.M. Weber, A.J. Ryan, ATM and ATR as therapeutic targets in cancer, Pharmacology & Therapeutics 149 (2015) 124-138.
[57] C. Karlsson-Rosenthal, J.B.A. Millar, Cdc25: mechanisms of checkpoint inhibition and recovery, Trends in cell biology 16(6) (2006) 285-292.
[58] K. Liu, M. Zheng, R. Lu, J. Du, Q. Zhao, Z. Li, Y. Li, S. Zhang, The role of CDC25C in cell cycle

912 regulation and clinical cancer therapy: a systematic review, Cancer cell international 20(1) (2020)
913 1-213.
914 [59] L.E. Giono, L. Resnick-Silverman, L.A. Carvajal, S. St Clair, J.J. Manfredi, Mdm2 promotes
915 Cdc25C protein degradation and delays cell cycle progression through the G2/M phase, Oncogene
916 36(49) (2017) 6762-6773.
917 [60] E. Perdiguero, A.R. Nebreda, Regulation of Cdc25C Activity During the Meiotic G2/M
918 Transition, Cell cycle (Georgetown, Tex.) 3(6) (2004) 731-735.
919 [61] L.T. Vassilev, Cell Cycle Synchronization at the G 2 /M Phase Border by Reversible Inhibition of
920 CDK1, Cell cycle (Georgetown, Tex.) 5(22) (2006) 2555-2556.
921 [62] W.R. Taylor, G.R. Stark, Regulation of the G2/M transition by p53, Oncogene 20(15) (2001)
922 1803-1815.
923 [63] M.B. Kastan, O. Onyekwere, D. Sidransky, B. Vogelstein, R.W. Craig, Participation of p53
924 protein in the cellular response to DNA damage, Cancer research (Chicago, Ill.) 51(23) (1991) 6304-
925 6311.
926 [64] E.S. Helton, X. Chen, p53 modulation of the DNA damage response, Journal of cellular
927 biochemistry 100(4) (2007) 883-896.
928 [65] X. Sun, P.D. Kaufman, Ki-67: more than a proliferation marker, Chromosoma 127(2) (2018)
929 175-186.
930 [66] S. Watanabe, S. Kawamoto, N. Ohtani, E. Hara, Impact of senescence-associated secretory
931 phenotype and its potential as a therapeutic target for senescence-associated diseases, Cancer
932 science 108(4) (2017) 563-569.
933 [67] R. Kumari, P. Jat, Mechanisms of Cellular Senescence: Cell Cycle Arrest and Senescence
934 Associated Secretory Phenotype, Frontiers in cell and developmental biology 9 (2021) 645593-
935 645593.
936 [68] G. Bollag, P. Hirth, J. Tsai, J. Zhang, P.N. Ibrahim, H. Cho, W. Spevak, C. Zhang, Y. Zhang, G.
937 Habets, E.A. Burton, B. Wong, G. Tsang, B.L. West, B. Powell, R. Shellooe, A. Marimuthu, H. Nguyen,
938 K.Y.J. Zhang, D.R. Artis, J. Schlessinger, F. Su, B. Higgins, R. Iyer, K. D'Andrea, A. Koehler, M. Stumm,
939 P.S. Lin, R.J. Lee, J. Grippo, I. Puzanov, K.B. Kim, A. Ribas, G.A. McArthur, J.A. Sosman, P.B. Chapman,
940 K.T. Flaherty, X. Xu, K.L. Nathanson, K. Nolop, Clinical efficacy of a RAF inhibitor needs broad target
941 blockade in BRAF-mutant melanoma, Nature 467(7315) (2010) 596-599.
942 [69] P.A.M.D. Ascierto, D.P. Schadendorf, C.P. Berking, S.S.P. Agarwala, C.M.L.M.D. van Herpen,
943 P.M.D. Queirolo, C.U.M.D. Blank, A.P. Hauschild, J.T.M.D. Beck, A.P. St-Pierre, F.M. Niazi, S.P.
944 Wandel, M.M.D. Peters, A.M.D. Zubel, R.P. Dummer, MEK162 for patients with advanced
945 melanoma harbouring NRAS or Val600 BRAF mutations: a non-randomised, open-label phase 2
946 study, The lancet oncology 14(3) (2013) 249-256.
947 [70] S.V. Bhagwat, W.T. McMillen, S. Cai, B. Zhao, M. Whitesell, W. Shen, L. Kindler, R.S. Flack, W.
948 Wu, B. Anderson, Y. Zhai, X.J. Yuan, M. Pogue, R.D. van Horn, X. Rao, D. McCann, A.J. Dropsey, J.
949 Manro, J. Walgren, E. Yuen, M.J. Rodriguez, G.D. Plowman, R.V. Tiu, S. Joseph, S.B. Peng, ERK
950 inhibitor LY3214996 targets ERK pathway–driven cancers: A therapeutic approach toward
951 precision medicine, Molecular cancer therapeutics 19(2) (2020) 325-336.
952 [71] H. Hirai, H. Sootome, Y. Nakatsuru, K. Miyama, S. Taguchi, K. Tsujioka, Y. Ueno, H. Hatch, P.K.

Majumder, B.S. Pan, H. Kotani, MK-2206, an allosteric akt inhibitor, enhances antitumor efficacy by standard chemotherapeutic agents or molecular targeted drugs in vitro and in vivo, Molecular cancer therapeutics 9(7) (2010) 1956-1967.
[72] B.D. Kahan, J.S. Camardo, Rapamycin: Clinical results and future opportunities, Transplantation 72(7) (2001) 1181-1193.
[73] Y. Zhang, L. Wu, Z. Wang, J. Wang, S. Roychoudhury, B. Tomasik, G. Wu, G. Wang, X. Rao, R. Zhou, Replication Stress: A Review of Novel Targets to Enhance Radiosensitivity-From Bench to Clinic, Frontiers in oncology 12 (2022) 838637-838637.
[74] R.D. Carruthers, S.U. Ahmed, S. Ramachandran, K. Strathdee, K.M. Kurian, A. Hedley, N. Gomez-Roman, G. Kalna, M. Neilson, L. Gilmour, K.H. Stevenson, E.M. Hammond, A.J. Chalmers, Replication stress drives constitutive activation of the DNA damage response and radioresistance in glioblastoma stem-like cells, Cancer research (Chicago, Ill.) 78(17) (2018) 5060-5071.
[75] C. Bruhn, M. Foiani, A model of DNA damage response activation at stalled replication forks by SPRTN, Nature communications 10(1) (2019) 5671-3.
[76] A. Arcaro, A.S. Guerreiro, The Phosphoinositide 3-Kinase Pathway in Human Cancer: Genetic Alterations and Therapeutic Implications, Current genomics 8(5) (2007) 271-306.
[77] F.H. Stootman, D.M. Fisher, A. Rodger, J.R. Aldrich-Wright, Improved curve fitting procedures to determine equilibrium binding constants, Analyst (London) 131(10) (2006) 1145-1151.
[78] X. Xie, B. Choi, E. Largy, R. Guillot, A. Granzhan, M.P. Teulade-Fichou, Asymmetric distyrylpyridinium dyes as red-emitting fluorescent probes for quadruplex DNA, Chemistry 19(4) (2013) 1214-26.

List of Figure Captions

Figure 1. *In vitro* study of the interaction between B3C and different nucleic acid sequences. (A) Fluorescence titration experiments. The enhanced fluorescence intensity monitored at 595 nm to study the interaction between **B3C** with various G4-RNA, non G4-RNA, G4-DNA, and non-G4 DNA in a pH 7.4 Tris-HCl buffer (10 mM) containing 60 mM KCl. The ligand concentration was 2 μM with nucleic acid substrates at 10 μM. (B) Fluorescence titration spectrum of 2 μM **B3C** with NRAS G4-RNA in a pH 7.4 Tris-HCl buffer (10 mM) containing 60 mM KCl. (C) CD spectrum of NRAS G4-RNA with or without **B3C** (25 μM) in a Tris-HCl buffer (10 mM, pH 7.4) without KCl. (D) CD melting curves for NRAS G4-RNA with or without the addition of **B3C** in a pH 7.4 Tris-HCl buffer (10 mM) containing 60 mM KCl (E) ITC study for the interaction between **B3C** and NRAS G4-RNA in a pH 7.4 KH_2PO_4 buffer solution (25 mM) containing 60 mM KCl. (F) The zwitterionic structure of **B3C**.

Figure 2. Confocal imaging of B3C in HeLa cell. (A) Confocal live-cell imaging **B3C** (5 μM, 15 mins) and Hoechst 33342 (2 μM, 10 mins). (B) Confocal co-localization live-cell imaging of **B3C** (5 μM, 15 mins) and MitoTacker Deep Red (30 nM, 30 mins). (C) Immunofluorescent co-localization imaging of **B3C** (5 μM, 15 mins) and lysosome associate membrane protein 1 (LAMP-1). (D) Immunofluorescent co-localization imaging of **B3C** (5 μM, 15 mins) and G4 specific antibody, BG4. (E) Confocal enzymatic digestion imaging of fixed HeLa cells with **B3C** (5 μM, 15 mins) and DAPI (2 μM, 10 mins) with or without RNase A and DNase I treatment. (F) Confocal competitive imaging of **B3C** (5 μM, 15 mins) and Hoechst 33342 (2 μM, 10 mins) with or without the addition of 5 and 10 μM **CarboxyPDS** (2 h).

Figure 3. Cellular study on the expression of mRNA and proteins after the treatment of B3C on HeLa cells. (A) The relative transcription of TERRA ncRNA, TRF2 mRNA, NRAS mRNA, KRAS mRNA, and VEGF mRNA in HeLa cells treated with **B3C** (0, 5, 10, and 20 μM) for 48 h, and GAPDH was used as the endogenous control (N= 3, mean ± SD). (B) Western blots assay to determine the translation of NRAS, TRF2, KRAS, VEGFA, γ-H2AX, t-p53, phos-p53 (Ser15), and β-actin in HeLa cells treated with **B3C** (0, 5, 10 and 20 μM) for 48 h. (C) The relative proteins expression of HeLa cells after the treatments with **B3C** of different concentration (N =3, mean ± SD). (D) Relative luciferase activity (ratio of *Renilla* luciferase activity to firefly luciferase activity) in psi-CHECK2 vectors containing the NRAS mRNA G4 (WT) or mutated sequence (Mut) upon the treatment of **B3C** (0, 5, 10, and 20 μM) for 24 h. (E) Recruitment of DHX36 to the NRAS mRNA upon the treatment of **B3C** (20 μM) in HeLa cells in the RIP assay. (F) RNA sequencing analysis in HeLa treated without or with **B3C** for 48 h. Details of gene expression data were given in Figure S17 to S19 in Supporting Information.

Figure 4. The study on induction of DNA damage and the activation of DNA Damage Response (DDR) after the treatment of B3C on HeLa cells. (A) Comet assay analysis of DNA damage in HeLa cells after 48 h of treatment **B3C** (10 and 20 μM). (B) Schematic diagram of the proteins in ATR and ATM DNA-damage pathways. (C) Western blots assay to determine the activation of DDR pathway by the translation of t-ATR, p-ATR (Ser428), t-CHK1, p-CHK1 (Ser345), t-ATM, p-ATM (Ser1981), t-CHK2, p-CHK2 (Thr68), t-CDC25C, p-CDC25C (Ser216), t-CDK1, p-CDK1 (Thr14/Thy15) and GAPDH in HeLa cells treated with **B3C** (0, 5, 10 and 20 μM) for 48 h. (D) The relative proteins expression of HeLa cells after the treatments with **B3C** of different concentration (N =3, mean ± SD).

Figure 5. The mechanism of B3C in the inhibition of HeLa cell growth and proliferation. (A) The percentage of HeLa cells in different phases in the cell cycle after the treatments with **B3C** of different concentration (N=3, mean ± SD) for 48 h. (B) Analysis of cell proliferation of HeLa cells by in vitro colony formation assay after the treatment of **B3C** (0, 2, and 4 μM) for 10 days. (C) Analysis of HeLa cells migration by in vitro wound healing assay after the treatment of **B3C** (20 μM) for 48 h. (D) Immunofluorescent imaging of Ki-67 to study the cell proliferation of HeLa cells after **B3C** treatment (0, 5, 10, and 20 μM) for 48 h. (E) The percentage of apoptotic HeLa cells after the treatments with **B3C** of different concentration (N=3, mean ± SD) for 48h. (F) Apoptosis analysis by western blotting to determine the expression of apoptotic proteins, cleaved PARP-1, cleaved caspase-3 in HeLa cells after treating with **B3C** (0, 5, 10 and 20 μM) for 48 h. (G) The percentage of apoptotic HeLa cells after the treatments with **B3C** of different concentration (N=3, mean ± SD).

Figure 6. The study on the induction of senescence on B3C treated HeLa cells and the synergetic effects of the combination of B3C and clinical PI3K inhibitor. (A) SA-β-gal assays to investigate the effects of **B3C** on cell senescence of HeLa cells. (B) The relative transcription of SASP related mRNA, *IL-1α, IL-6, and IL-8* in HeLa cells treated with **B3C** (0, 5, 10, and 20 μM) for 48 h, and GAPDH was used as the endogenous control (N=3, mean ± SD). (C) The relative proteins expression of SASP related proteins, IL-1α, IL-6, and IL-8 in HeLa cells after the treatments with **B3C** of different concentration (N=3, mean±SD). (D) The cell growth inhibition of **B3C** alone, PI3Ki alone, and **B3C**-PI3Ki combination (10 and 20 μM PI3Ki) to HeLa cells for 48h, which were measured by MTT assay. (E) Synergy heatmap showing the combination index (CI) for the cells treated **B3C** with PI3Ki at different combinations.